Stegemann Jan P (Orcid ID: 0000-0002-7989-7222)

Fabrication and Characterization of Osteogenic Function of Progenitor Cell-Laden Gelatin Microcarriers

Chukwuma E. Nweke and Jan P. Stegemann*

Department of Biomedical Engineering, University of Michigan, Ann Arbor

* Corresponding Author: Department of Biomedical Engineering

Ann and Robert H. Lurie Biomedical Engineering Building

University of Michigan

1101 Beal Avenue, Ann Arbor, MI, 48109

Email: jpsteg@umich.edu

Running Title: Gelatin Microcarriers for Cell Delivery

This is the author manuscript accepted for publication and has undergone full peer review but has not been through the copyediting, typesetting, pagination and proofreading process, which may lead to differences between this version and the Version of Record. Please cite this article as doi: 10.1002/jbm.b.34998

Abstract

Biomaterial-based bone regeneration strategies often include a cellular component to accelerate healing. Modular approaches have the potential for minimally-invasive delivery and the ability to conformally fill complex defects. In this study, spherical gelatin microparticles were fabricated via water-in-oil emulsification and were subsequently crosslinked with genipin. Microparticle diameter depended on impeller geometry, and increased stirring rates consistently produced smaller particles with narrower size distributions. Increasing the concentration of gelatin resulted in larger particles with a broader size distribution. Viscoelastic characterization showed that increased gelatin concentration produced stiffer matrices, though the mechanical properties at lower gelatin concentration were more stable across strain rate. Microparticles of 6.0 % wt/vol gelatin were then applied as microcarriers for packed-bed culture of human mesenchymal stromal cells (MSC) at seeding densities of 5.0×10^3, 2.5×10^4, or 5.0×10^4 cells/cm^2 of surface area, in either control or osteogenic medium. Cell viability was uniformly high (>90%) across seeding densities over 22 days in culture. MSC number stayed approximately constant in the 5.0×10^3 and 2.5×10^4 cells/cm^2 samples, while it dropped over time at 5.0×10^4 cells/cm^2. Alkaline phosphatase activity was significantly upregulated in osteogenic conditions relative to controls at day 15, and absolute calcium deposition was strongly induced by days 15 and 22. However, calcium deposition per cell was highest in the lowest cell density, suggesting an inhibitory effect of high cell numbers. These results show that genipin-crosslinked gelatin microcarriers can be reproducibly fabricated and used as microcarriers for progenitor cells, which may have utility in treating large and complex bone defects.

Introduction

Trauma and disease-induced bone fractures can be severely debilitating, in particular when the structure of the local microenvironment and/or cell populations are disrupted. Inhibition of bone regeneration by injury or disease can result in significant clinical morbidity, including delayed bone healing and non-unions [1, 2]. The field of biomaterials science has addressed these issues through the development of a variety of promising approaches to improving bone healing outcomes. Many of these approaches apply the conventional tissue engineering paradigm of combining osteogenic cells with a supportive biomaterial scaffold, in some cases in conjunction with controlled factor release, to guide and potentiate bone regeneration [3, 4]. Mesenchymal stromal cells (MSC) are often used in these applications because of their demonstrated involvement in the regeneration of bone [5, 6], as well as their putative paracrine and immunomodulatory effects [7, 8]. Cell-based approaches are particularly promising because only cells can create new bone, and in situations where regenerative cells are absent from the wound site they must either be recruited or provided exogenously [9, 10].

There is increasing interest in the development of biomaterials-based modular tissue engineering systems, in which discrete units of material and/or engineered tissues are delivered to achieve a specific function. Modular approaches allow minimally-invasive delivery, and even complex defects can be conformally filled [11, 12]. The modular strategy also allows different types of tissue constructs to be combined to form complex and multiphasic engineered tissues [13, 14]. To date, the main approaches for creating therapeutic bone fillers have used larger particulates, often auto- or allograft, with dimensions on the order of millimeters [15, 16]. However, the potential of micron-range colloidal particulates to enhance cellular development and tissue-specific function is now being investigated more widely [13]. Particles in this size range are commonly called microcarriers, and are designed to maximize their capacity for attachment of cell populations, and for use as a cell culture and delivery method. Through careful biomaterial selection and fabrication, microcarriers can be created with tailored combinations of bioactivity, rigidity, and degradability.

In general, the microcarrier format offers a number of advantages over other cell culture and delivery approaches. A variety of microcarrier types are used routinely in the biotechnology industry [17, 18], and there is a well-developed body of science on process control, aseptic processing, and quality assurance. Microcarriers provide a very high surface area to volume ratio and therefore allow large cell populations to be supported in relatively small volumes: it is remarkable to consider that 10 mL of a concentrated paste of 150 μm-diameter microcarriers could support almost 250 million cells. Microcarriers can also be cultured in suspension, which greatly simplifies their maintenance, harvesting and potential use for cell transplantation. Importantly, cells cultured on microcarriers can be collected without the need for trypsinization and removal from their substrate, and intact populations of microcarriers can therefore be used for cell delivery, e.g. as a cell-containing tissue filler. Such use maintains the very important cell-matrix and cell-cell contacts that are critical to tissue survival, engraftment, and development post-transplantation. In addition, cell delivery in a packed-bed geometry of concentrated microcarriers promotes

diffusion-based and/or microvasculature-enabled perfusion of nutrients to and from the transplanted cells in ischemic environments.

Microcarriers for bone regeneration commonly use biomaterials with established biological relevance [19, 20], including collagen, gelatin, calcium phosphates, apatites, bioactive glasses, and calcium carbonates [21, 22]. Typically, microspheres of such cytocompatible materials are generated through the batch emulsification or pinched flow droplet formation of an aqueous polymer solution phase into a surrounding nonpolar phase (recently reviewed in [13]). Batch-emulsification provides the benefit of rapid microparticle production, but at the cost of greater size polydispersity. Particle size and size distribution can be modulated to some degree by varying the viscosity of the continuous phase, the rate of emulsification, and the impeller geometry, as well as by the addition of surfactants and post-production filtration [23, 24]. In contrast, microfluidic or flow-focusing techniques are capable of generating particles with a narrow size distribution; however, the rate of production is comparatively low [25, 26].

Gelatin and other collagen-derived materials have been used extensively as base materials for microcarriers due to their broad availability, ease of processing, and generally excellent cytocompatibility. There is a rich literature on the use of collagen and gelatin microparticles as cell carriers, and several commercial products are available, including collagen Cellagen [27], gelatin Cultispher®-S [28, 29], and porous gelatin-coated dextran Cytodex®-3 microcarriers. The fabrication of collagen [23, 30] and gelatin [31-33, 34, 35, 36] microparticles has been demonstrated using bulk emulsification [37, 38], microfluidics [39], coacervation [40], and sol-gel synthesis [12]. In some cases these microcarriers are augmented with other macromolecules such as chitosan [41] or silk fibroin [25, 39], or with a mineral phase such as tricalcium phosphate [15, 30], calcium-deficient hydroxyapatite [42, 43], or hydroxyapatite [44, 38].

Collagen and collagen-peptides foster the attachment and reorganization by many cell types, including a variety of progenitor cells known to be involved in bone formation. Additionally, these materials are autocatalytically, thermally, or chemically-crosslinkable at room temperature and in physiological conditions [30]. The mechanical properties of collagen-based materials can be further controlled through the addition or reduction of reinforcing agents. Such physical changes can in turn alter the osteogenic capacity of the substrate, as evidenced by changes in key phenotype markers, including alkaline phosphatase, osteocalcin, and calcium deposition. Gelatin in particular has found use in a number of bone defect filler applications, as a result of this material's low cost, ease of handling, and general cytocompatibility [15, 23, 27-29, 45-46]. Gelatin is available as a highly purified product, and consists of collagen polypeptides that are soluble in hot water. When cooled below 25 °C, the peptides form a hydrogel, which can be crosslinked to produce a stable matrix. These materials retain the cell-binding sites of native collagen, and therefore are excellent cell culture substrates.

In the current study, gelatin microparticles were fabricated through an oil-in-water emulsification method, with a focus on achieving a high production rate and a narrow population size distribution. The effect of impeller geometry, stirring rate, and gelatin concentration on the size and size distribution of gelatin microparticles was assessed. Formed microparticles were

subsequently crosslinked with genipin, a small molecule that imparts markedly less residual cytotoxicity to protein- and peptide-based matrices, relative to commonly used aldehyde crosslinkers [47]. The viscoelastic mechanical properties of the crosslinked gelatin matrices were assessed using shear rheometry. MSC were seeded onto select genipin-crosslinked gelatin microparticle formulations to create cell microcarriers consisting of osteoprogenitor cells attached to a peptide matrix. These microcarriers were cultured in a packed-bed geometry to loosely mimic how such particles can be delivered in bone defect-filling applications. The viability, proliferation, and differentiated state of the MSC were assessed over a period of three weeks in both control and osteogenic culture. Few previous studies have focused on the use if genipin-crosslinked gelatin microcarriers for osteogenesis, and most have been limited to shorter culture times [31-33]. The goal of the current study was to characterize the fabrication of genipin-crosslinked gelatin microcarriers and their capacity for support of bone cell maintenance, growth and differentiation, with an emphasis on the ability to promote osteogenic differentiation of human progenitor cells.

Materials and Methods

Materials

Type A (acid-treated porcine skin) 225 bloom strength gelatin was procured from Sigma Aldrich (St. Louis, MO, USA). A 100 cSt polydimethylsiloxane (PDMS) product was procured from Clearco Products (Bensalem, PA, USA). Pluronic® L101, a nonionic, difunctional, block copolymer surfactant, was procured from BASF Corporation (Vandalia, IL, USA). Genipin, a naturally-derived crosslinking agent, was procured from Wako Chemicals (Richmond, VA, USA).

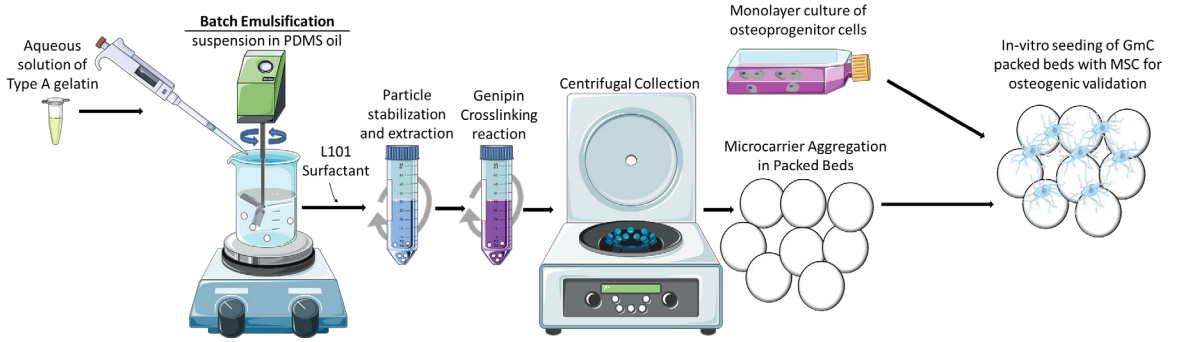

Figure 1: Schematic showing gelatin microcarrier production by water-in-oil emulsification and subsequent seeding with cells. Microcarriers in this study were composed of Type A gelatin crosslinked with genipin.

Generation of gelatin microcarriers

A water-in-oil emulsification process, illustrated schematically in **Figure 1**, was used to generate gelatin microscale droplets. Aliquots of 5.0 mL of the desired gelatin concentration (6.0, 10.0, or 14.0% (wt/vol) gelatin in PBS at pH 7.4) were equilibrated within a 37 °C water bath before dropwise addition to a stirred 50 mL PDMS oil bath held at 40 °C on a heated plate. The resultant emulsion was stirred at set rates of 250, 380, or 500 rpm with custom impellers. These

impeller designs are shown in **Figure 2** as: a radial-blade impeller with a 7 mm by 12.47 mm cross-section 35 mm-long blade and two dual-blade axial impellers with cylindrical blade diameters of 0.33 mm or 1.0 mm. While the radial-blade impeller has been used in previous studies, the axial impellers have been custom designed for the generation of microparticles used as microcarriers in this current study. After 5 minutes of stirring at 40 °C, using one of these three impellers, the resulting emulsion was transferred to a 4 °C ice bath and stirring was continued for an additional 30 minutes to allow microdroplet solidification. The resulting suspension of solid gelatin microparticles was mixed with PBS at 23 °C containing 0.01% (vol/vol) Pluronic L101 surfactant and centrifuged at 300 × G for 5 minutes to collect the gelatin microparticles and separate them from the PDMS phase [48]. Remaining surfactant solution was extracted from collected microparticles by re-suspension and washing in PBS for further processing.

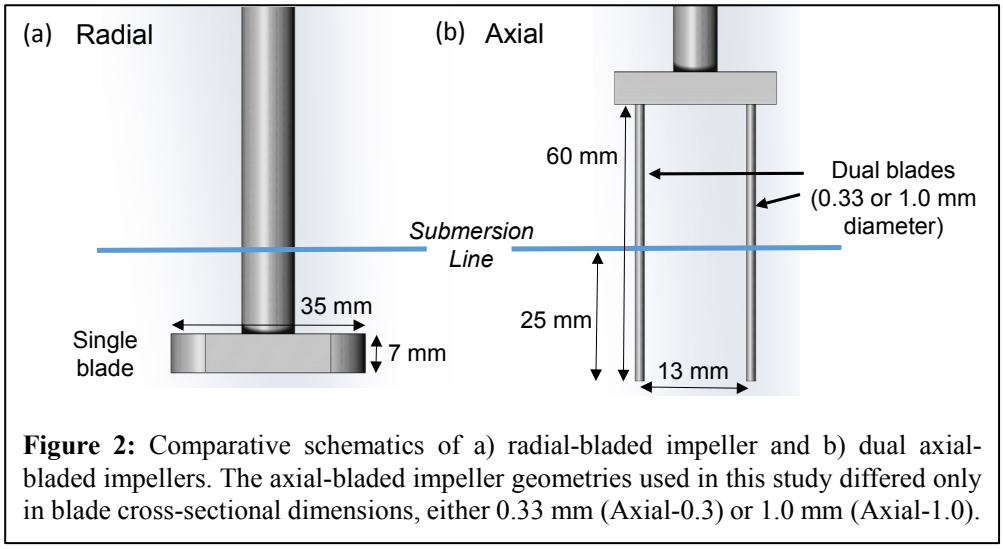

Figure 2: Comparative schematics of a) radial-bladed impeller and b) dual axial-bladed impellers. The axial-bladed impeller geometries used in this study differed only in blade cross-sectional dimensions, either 0.33 mm (Axial-0.3) or 1.0 mm (Axial-1.0).

Genipin crosslinking of gelatin microcarriers

Gelatin microparticles were admixed to 1.0% (wt/vol) genipin in PBS solution under continuous rotational suspension to allow crosslinking to occur. Degree of crosslinking was time-dependent and a mixing duration of 48 hours at 23 °C was used to allow total saturation of reactive amine groups [34]. Genipin creates crosslinks by catalyzing reactions between lysine residues on amine moieties of the gelatin molecule. Hydrogels crosslinked in this manner have been determined to reach a maximum degree of crosslinking of approximately 90 %, which imparts a mild red autofluorescence the gelatin material [35, 49]. The gelatin used in this study had a melting temperature of approximately 32 °C, such that crosslinking could be carried out at room temperature without fusion of particles. Crosslinked gelatin microcarriers (GmC) were washed successively in ethanol and deionized (DI) water to extract residual genipin. All microcarriers were subjected to 10 minutes of ethanol-submersion sterilization and UV sterilization (Sylvania UV-C 255 nm germicidal T8 30W lamp) before use.

Particle size analysis

General examination and characterization of the morphology of gelatin microparticles was accomplished using light microscopy. GmC micrographs were captured with an inverted phase contrast microscope and analyzed using NIS Elements viewer software (Nikon). Automated particle size measurement was performed using laser diffraction analysis (Malvern Mastersizer 2000S, Westborough, MA). Samples of microcarrier dispersions were suspended in DI water within the sample reservoir agitated at 1750 rpm. The count median diameter for GmC was measured until the recorded laser obscuration exceeded 5%. Using Mie light scattering theory, a gelatin refractive index of 1.52, and water's refractive index of 1.33, the particle analyzer calculated a distribution of spherical particle diameters by scanning 30,000 snapshots over a 30 second time-span. Data generated from automated particle analysis were used to graph particle size distributions and calculate population statistics. Histograms presented in this work use bins in which the bin labels represent the maximum size of the lower bin, which is also the minimum size of the next larger bin.

Mechanical characterization of gelatin materials

Rheological analysis was used to determine the impact of gelatin concentration on material mechanical properties. Gelatin hydrogels were characterized using a rotational rheometer (AR-G2, TA Instruments, Newcastle DE) with a Peltier temperature-controlled stage and 8 mm parallel plate measurement head. Measurements were taken at 25 °C on 10 mm diameter discoid samples of 6.0, 10.0, or 14.0% (wt/vol) gelatin at a pre-load of 0.5 N with a gap height of 3 mm. A 0.1-10 radian/second (rad/s) oscillating frequency sweep test was conducted at a constant oscillating strain of 0.1% to identify the linear viscoelastic region (LVER). A 0.1 - 10% oscillating strain sweep test was then administered at a constant oscillating frequency of 1 rad/s to establish a modulus-strain relationship for the specified concentrations of gelatin hydrogels. Finally, a 20 s time sweep test was administered at a constant oscillating frequency of 1 rad/s and constant oscillating strain of 0.1%.

Cell culture

Human bone marrow-derived mesenchymal stem cells (MSC, RoosterBio, Frederick MD) were expanded to passage 7 in defined growth medium (RoosterNourish^{TM}, RoosterBio, Frederick MD). Control medium (CTRL) consisted of Dulbecco's Modified Eagle's Medium (DMEM) supplemented with 10% (vol/vol) fetal bovine serum (FBS) and 1% (vol/vol) penicillin-streptomycin. Osteogenic (OST) medium was prepared by adjusting CTRL medium to final concentrations of 0.2 mM L-ascorbic acid 2-phosphate, 10 mM β-glycerophosphate, and 100 nM dexamethasone. All cell culture was performed in a standard incubator at 37 °C in a 5% CO_2. Upon reaching 70–80% confluence in T-175 polystyrene culture flasks, MSC were trypsinized and suspended in medium for seeding of GMC at cell densities of 5,000 MSC/cm^2 (5K/cm^2), 25,000 MSC/cm^2 (25K/cm^2), or 50,000 MSC/cm^2 (50K/cm^2). GmC used in cell culture experiments were generated using an Axial-1.0 impeller at 500 rpm, resulting in an average GMC diameter of 177.3

μm. GMC were cultured in packed beds in a conical tube to loosely simulate how microcarriers would be assembled if used as a bone void-filling material. Nutrient medium was changed every 3-4 days over the span of a three-week culture period.

Cell viability, number, ALP activity, and calcium deposition

On day 1 after seeding, and subsequently on day 8, day 15, and day 22 of culture, MSC were assayed for DNA content, ALP activity, and calcium deposition. These assays were used to characterize the number, proliferation rate, and differentiated state of the MSC. Additionally, vital staining was performed on days 8, 15, and 22 to determine the viability, general shape, and distribution of MSC in microcarrier culture.

Packed-beds of MSC-loaded microcarriers were transferred to 24-well plates for visual inspection and were incubated with 0.1% (vol/vol) calcein AM and 0.1% (vol/vol) ethidium homodimer in DMEM for 45 minutes prior to rinsing and suspension in PBS. Both fluorescence and bright-field imaging on an inverted microscope were used to assess cell viability and morphology. Live cells were captured in the green fluorescence channel while the red channel of the same field of view was imaged to capture any dead cells and microcarrier autofluorescence. Corresponding bright-field images of these fields captured all cells and microcarriers.

The quantity of cellular DNA in samples was assayed as a measure of relative cell numbers, which were used to normalize ALP activity and calcium deposition, using the commercially available Quanti-iT™ PicoGreen double-stranded DNA assay kit kit (Invitrogen, Grand Island, NY) as described previously [36]. Briefly, total DNA was isolated from packed-bed culture samples through solubilization in 0.1% (wt/vol) sodium dodecyl sulfate 10 mM Tris-HCL solution (0.1%SDS TBS) adjusted to a pH of 7.5. Samples were subsequently centrifuged at 10,000 × G for 10 minutes before aspiration of supernatants for further use in quantifying DNA content by PicoGreen assay using the manufacturer's protocol and reagents. Briefly, lysate samples, alongside reference samples of Lambda-DNA standards, were admixed with 0.5% (vol/vol) PicoGreen 1mM ethylenediaminetetraacetic acid (EDTA) TBS for 5 minutes of reaction time. Fluorescence signal from each reacted sample, pipetted into a 96-well plate, was read with an excitation wavelength of 485 nm at an emission wavelength of 528 nm.

ALP activity was quantified as described previously [36] by first lysing MSC in 0.1 % SDS TBS, centrifuging at 10,000 × G for 10 minutes, and then collecting the respective supernatants. Sample supernatants were each admixed with 1.5 M 2-amino-2-methylpropanol-buffered 5 mM p-nitrophenyl phosphate substrate solution in a 96-well plate for 30 minutes of reaction on shaker plate. This reaction was stopped with the addition of 3.0 N NaOH to all sample wells. Sample absorbance was measured at 405 nm.

Calcium deposition was measured using an orthocresolphthalein complex one (OCPC) method described in earlier studies [50, 51]. Briefly, sample sediments from 10,000 × G centrifugation were digested in 1.0 N acetic acid overnight on a 37ºC shaker plate. These were each then admixed with a 5:5:2:88 volume ratio blend of 14.8 M ethanolamine-boric acid buffer (pH 11), 1 mg/ml OCPC solution, 50 mg/ml 8-hydroxyquinoline in 95% ethanol solution, and deionized water in a

96-well plate for 10 minutes of reaction on shaker plate. Sample absorbance was then measured at 575 nm.

Statistical analysis

Microcarrier sizes, mechanical data, ALP activities, calcium levels, and DNA yields are all reported as numerical mean ± standard deviation. For these data sets, groups were compared and analyzed by ANOVA and t-test. A resulting F-value of greater than F-critical and a p-value of less than 0.05 between groups were considered statistically significant.

Results and Discussion

Gelatin microparticle morphology and size

The effect of impeller geometry and rotation speed on the morphology, average size, and size distribution of gelatin microparticles was assessed both through optical imaging and automated particle size analysis. All formulations of batch-emulsified gelatin microparticles exhibited highly spheroidal geometries with regular borders and visually smooth surfaces. The diameter of microcarriers is functionally significant since it determines the surface area available for cell attachment on each particle. The size distribution of a population of microcarriers is important because it determines the achievable packing density of microparticles [52, 53], as the well as the overall surface area available for cell attachment.

Figure 3 shows the effect of impeller geometry on microparticle size using a rotational speed of 500 rpm, using a 6.0 % wt/vol gelatin matrix. Panels a-c show images of the produced microparticles and the corresponding size histograms. Microparticles generated by the radial impeller, displayed a relatively monodisperse size distribution dominated by very small gelatin particles (6.7±0.3 μm). This impeller geometry was used in previous studies [34-36] to create very small (6-21 μm diameter) microspheres designed for growth factor delivery. However, microcarriers designed as platforms for cell culture and delivery require sufficient surface area to support cell attachment, differentiation, and growth. Therefore, we experimented with other impeller geometries to create microcarriers of appropriate size and size distribution.

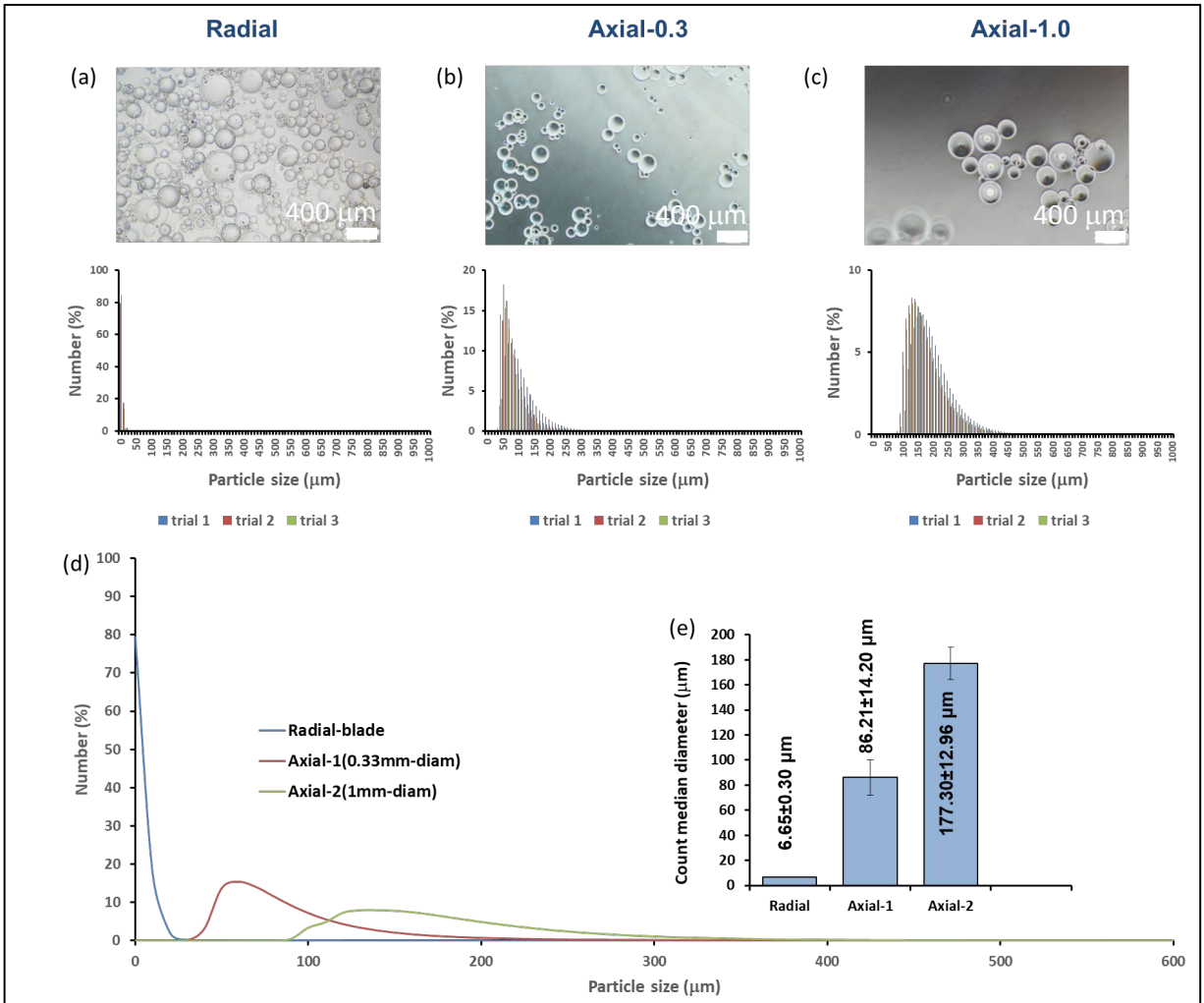

Figure 3: Effect of impeller geometry on microparticle size using a stirring rate of 500 rpm. Upper panels show brightfield optical microscopy and batch-to-batch size distribution of microparticles formed by a) radial-blade, b) 0.33 mm diameter axial-blade, and c) 1.0 mm diameter axial-blade impeller geometries. Scale bars represent 400 µm. Aggregate data are presented as d) representative size distributions, and e) median ± standard deviation for each impeller geometry.

The two axial impeller geometries that were investigated differed in the diameter of the impeller blade: the Axial-0.3 configuration used 0.33 mm diameter blades, while the Axial-1.0 version used 1.0 mm diameter blades. Axial blade impellers produced larger particles at the same rotation speed, relative to the radial impeller. The Axial-0.3 impeller created GmC with median diameters of 86.2 ± 14.2 µm, while the Axial-1.0 configuration produced microcarriers with median diameters of 177.3 ± 13.0 µm. Batch to batch reproducibility was very high for all impeller types (**Supplemental Figures S1, S2**). The error bars in Figures 3-6 represent the variation in average particle size between batches at the same fabrication conditions, further showing the repeatability between batches. The histograms in panel (d) of Figs 3-6 show the the variation of particle size within a given batch, since they show the entire population size distribution. A comparison across all impeller geometries (Fig. 3d) shows the distinct population size distribution

produced by each impeller type at a single rotational speed. Microparticle populations produced by the radial configuration were generally too small for use as cellular microcarriers, and therefore subsequent experiments were performed with axial-blade impellers.

The effect of impeller rotation speed was further examined using the axial blade configuration, again using a 6.0 % wt/vol gelatin matrix. Increasing rotation speed of the Axial-1.0 impeller from 250 rpm to 380 rpm to 500 rpm produced microparticles with count median diameters of 341.7 ± 16.9 µm, 222.0 ± 4.4 µm, and 177.3 ± 13.0 µm, respectively, as shown in **Figure 4**. The population size polydispersity decreased moderately with increasing impeller rate, as shown by the histograms of particle size (Fig. 4d) and aggregate sizing data (Fig. 4e). A similar study using the Axial-0.3 impeller resulted in median microparticle diameters of 173.2 ± 9.4 µm, 139.1 ± 5.8 µm, and 86.2 ± 14.2 µm, at 250, 380 and 500 rpm, as shown in **Figure 5**. The size distribution became narrower at the highest impeller rate and this impeller configuration resulted reproducible microcarrier batches in the general size range of 100-200 µm in diameter, which has been shown to be supportive of osteogenic activity of progenitor cells [54, 55]. Importantly, this size of microparticles is able to support attachment of multiple cells (50-100 per microcarrier, depending on size) and can also be injected through a needle as small as 21 gauge (inner diameter ~500 µm without damage.

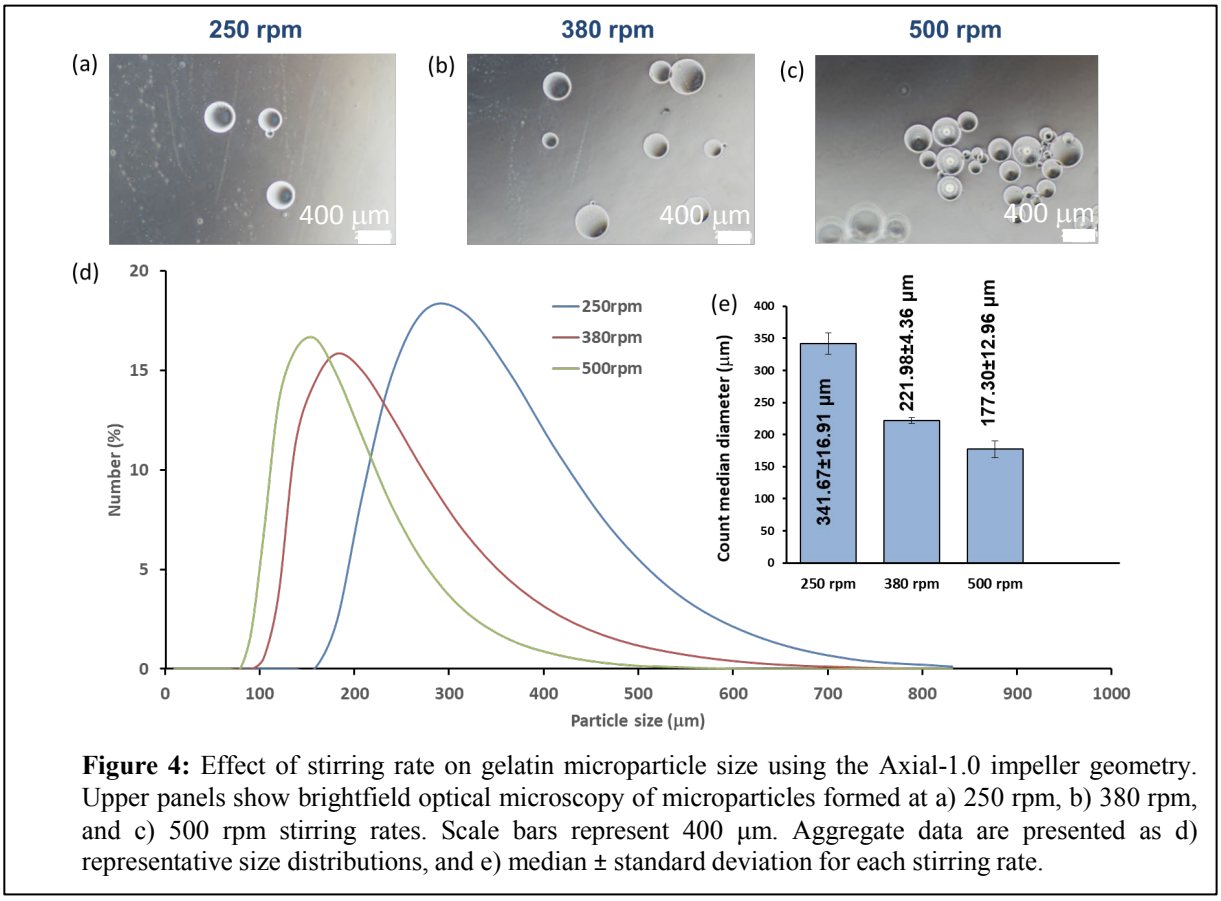

Figure 4: Effect of stirring rate on gelatin microparticle size using the Axial-1.0 impeller geometry. Upper panels show brightfield optical microscopy of microparticles formed at a) 250 rpm, b) 380 rpm, and c) 500 rpm stirring rates. Scale bars represent 400 µm. Aggregate data are presented as d) representative size distributions, and e) median ± standard deviation for each stirring rate.

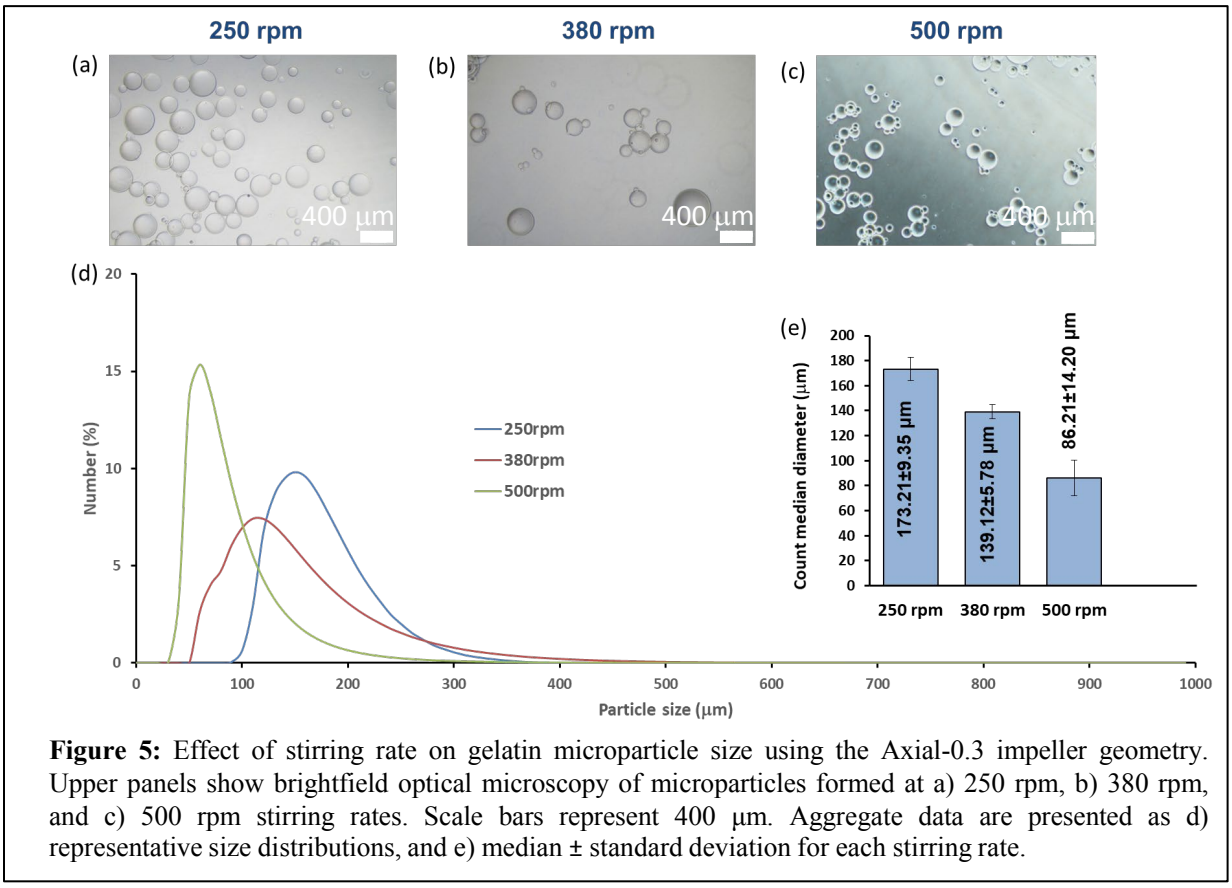

Figure 5: Effect of stirring rate on gelatin microparticle size using the Axial-0.3 impeller geometry. Upper panels show brightfield optical microscopy of microparticles formed at a) 250 rpm, b) 380 rpm, and c) 500 rpm stirring rates. Scale bars represent 400 µm. Aggregate data are presented as d) representative size distributions, and e) median ± standard deviation for each stirring rate.

Figure 6 shows the effects of gelatin concentration on the size of gelatin microparticles created using the Axial-0.3 impeller at a stirring speed of 500 rpm. The microparticles produced were similar in visual appearance (Fig. 6a-c), with a smooth and spherical morphology. Increasing the concentration of gelatin base material from 6.0 % to 10.0 % and 14.0 % (wt/vol) resulted in decreased polydispersity of the microparticle population, as shown by the histogram of the particle size distribution (Fig. 6d). Increasing gelatin concentration also resulted in a clear increasing trend in median particle size, with median diameters of 86.2 ± 14.2, 122.7 ± 4.1 µm, and 149.6 ± 6.2 µm, respectively, as shown in the aggregate population data (Fig. 6e).

In general, microparticle size exhibited a positive correlation with the quantity of dissolved solids and a negative correlation with the rate of stirring during emulsification. Additionally, these results suggested a negative correlation between the dissolved solids quantity and the population size polydispersity of the generated microparticle batch. These relationships provide flexibility when designing microcarriers for particular applications. In other studies, surfactants have been employed during emulsification in efforts to achieve greater control over size distribution, though their effect has generally not been strong and there can be concern about the effect on cell viability and function [23, 38, 40]. In the present study, microparticles were made without surfactants in the range of approximately 10-350 µm in diameter, depending on the impeller geometry, stirring rate, and matrix composition. It should be noted that gelatin concentrations as low as 2.0 % (wt/vol)

could be used to fabricate microparticles (data not shown); however, at low concentrations the resulting particles were irregular, non-spherical, and generally more fragile. Stable, spherical particles are preferred in cell delivery applications since their flow and packing properties are more predictable.

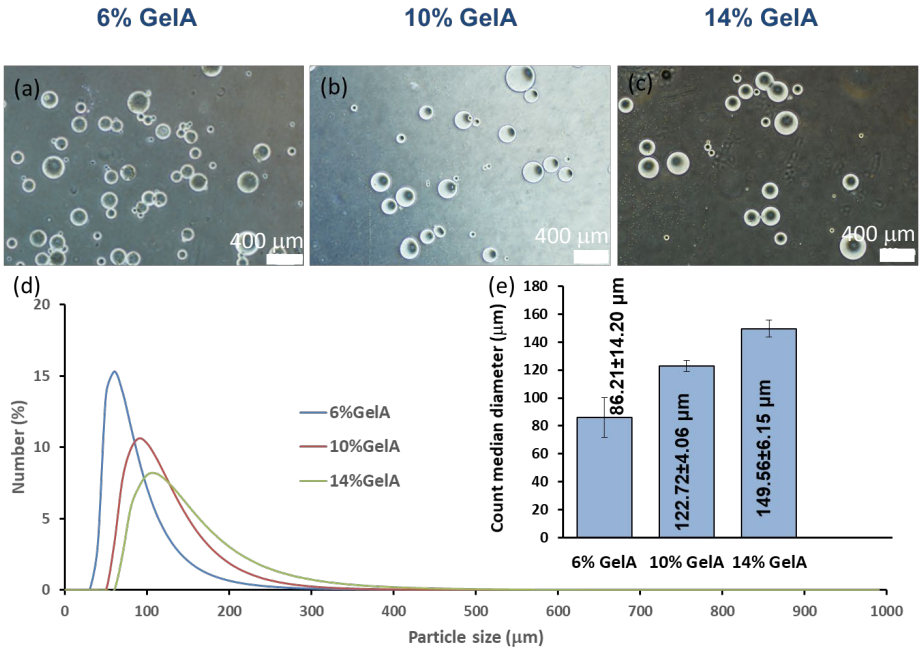

Figure 6: Effect of gelatin concentration on gelatin microparticle size using the Axial-0.3 impeller at 500 rpm. Upper panels show brightfield optical microscopy of microparticles formed at a) 6.0 % wt/vol, b) 10.0 % wt/vol, and c) 14.0 % wt/vol gelatin. Scale bars represent 400 µm. Aggregate data are presented as d) representative size distributions, and e) median ± standard deviation for each gelatin concentration.

Mechanical properties of gelatin materials

A range of mechanobiology studies have identified a link between cell culture substrate stiffness and the differentiation capacity of progenitor cells (reviewed recently in [56-59]). Gelatin is markedly less stiff than the natural collagen-hydroxyapatite composite of bone, but has been used widely as a cytocompatible and stable substrate for the culture of many cell types. Importantly, surfaces of stiffness well below that of the ceramic compounds in native bone have been shown to provide osteogenic enhancement to progenitor cells [60].

In the present study, the mechanical properties of gelatin at defined concentrations suitable for microparticle preparation were assessed using oscillatory shear rheometry, as shown in **Figure 7**. Hydrogels prepared with of 6.0 %, 10.0 %, and 14.0 % (wt/vol) gelatin were found to have shear storage moduli (G') of 34.7 ± 3.7 kPa, 45.8 ± 1.8 kPa, and 47.5 ± 3.7 kPa, respectively (Fig. 7a). The corresponding loss moduli (G") were 1.0 ± 0.2 kPa, 1.2 ± 0.1 kPa, and 2.0 ± 0.3 kPa, respectively (Fig. 7b). The direct positive correlation between gelatin content and shear modulus is presumably a result of greater polymer entanglement and interactions at higher solids content. A strain sweep from 0.1-10 % at 1 rad/s (Fig. 7c) showed that the storage modulus of 6.0 % gelatin

was markedly less sensitive to strain amplitude that that of the higher concentrations. This lower sensitivity to strain amplitude may result from an increased ratio between chemical and physical crosslinking, as chemical crosslinking is naturally less susceptible to physical deformation. The shear modulus determined in this study for 6.0 % (wt/vol) gelatin was similar to values previously reported to exhibit an osteogenic effect on similarly crosslinked collagenous substrates [56-59, 61]. We chose the 6.0 % gelatin for further study because of its consistent behavior across strain amplitudes, ease of preparation, and relevance to prior work [34-36, 62].

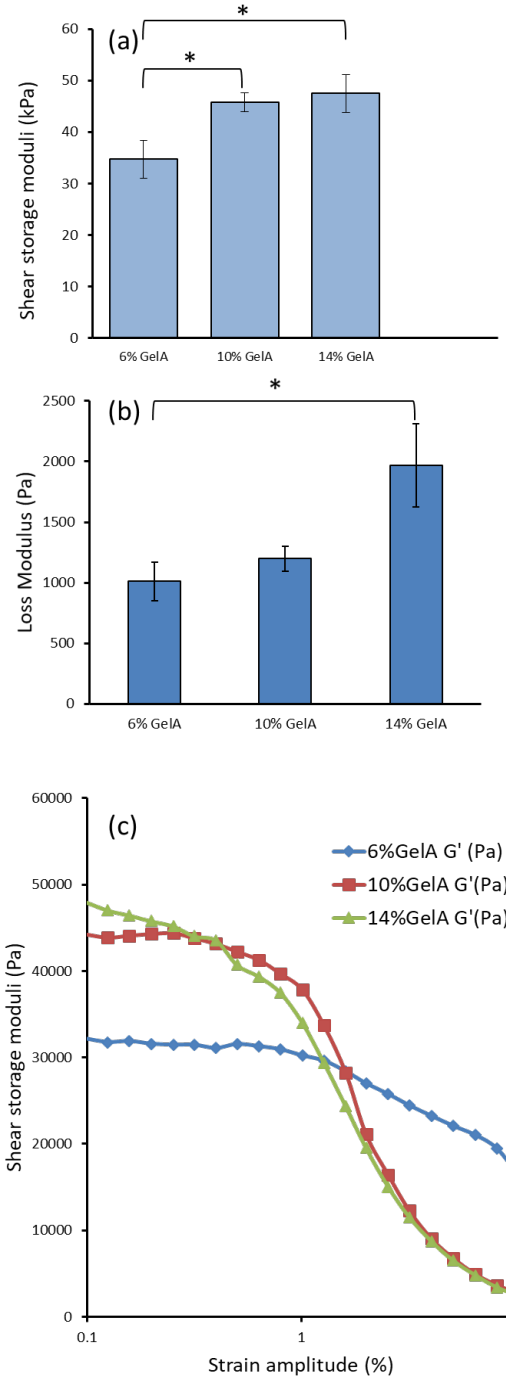

Figure 7: Mechanical properties of gelatin formulations determined using shear rheometry. Genipin-crosslinked gelatin materials were analyzed to determine the a) storage modulus, b) loss modulus, and c) effect of strain amplitude for formulations of 6.0, 10.0, and 14.0 % wt/vol. Brackets and associated stars indicate statistically significant differences ($p<0.05$).

Viability and osteogenic effect of seeding density in GmC culture

Figure 8 shows images of formed GmC that were seeded with MSC at nominal cell densities of 5,000 cells/cm^2 (5K/cm^2), 25,000 cells/cm^2 (25K/cm^2), or 50,000 cells/cm^2 (50K/cm^2) GMC created using an Axial-1.0 impeller at 500 rpm, resulting in an average diameter of 177.3 µm. GMC were cultured over 3 weeks in either control or osteogenic media. Brightfield images showed highly spherical particles with cells attached to their surfaces (Fig. 8a). The genipin-treated microparticles have a blue to purple pigmentation as a side product of the genipin-gelatin crosslinking reaction [31, 34, 36, 63, 64]. Viability staining of the cellular component allowed visualization of MSC under fluorescence microscopy. After two weeks of culture (Fig. 8b), cell viability assay in all sample conditions revealed highly viable cells, as evidenced by abundant green staining of living cells and very little red nuclear staining in dead cells. GmC fluoresce in the red channel due to autofluorescence caused by genipin crosslinking,

which facilitated identification of the substrate but had the potential to mask the red signal of dead cells. However, control experiments showed the presence of red-stained dead cell nuclei following ethanol treatment (**Figure S3**), which could be distinguished from the background gelatin autofluorescence.

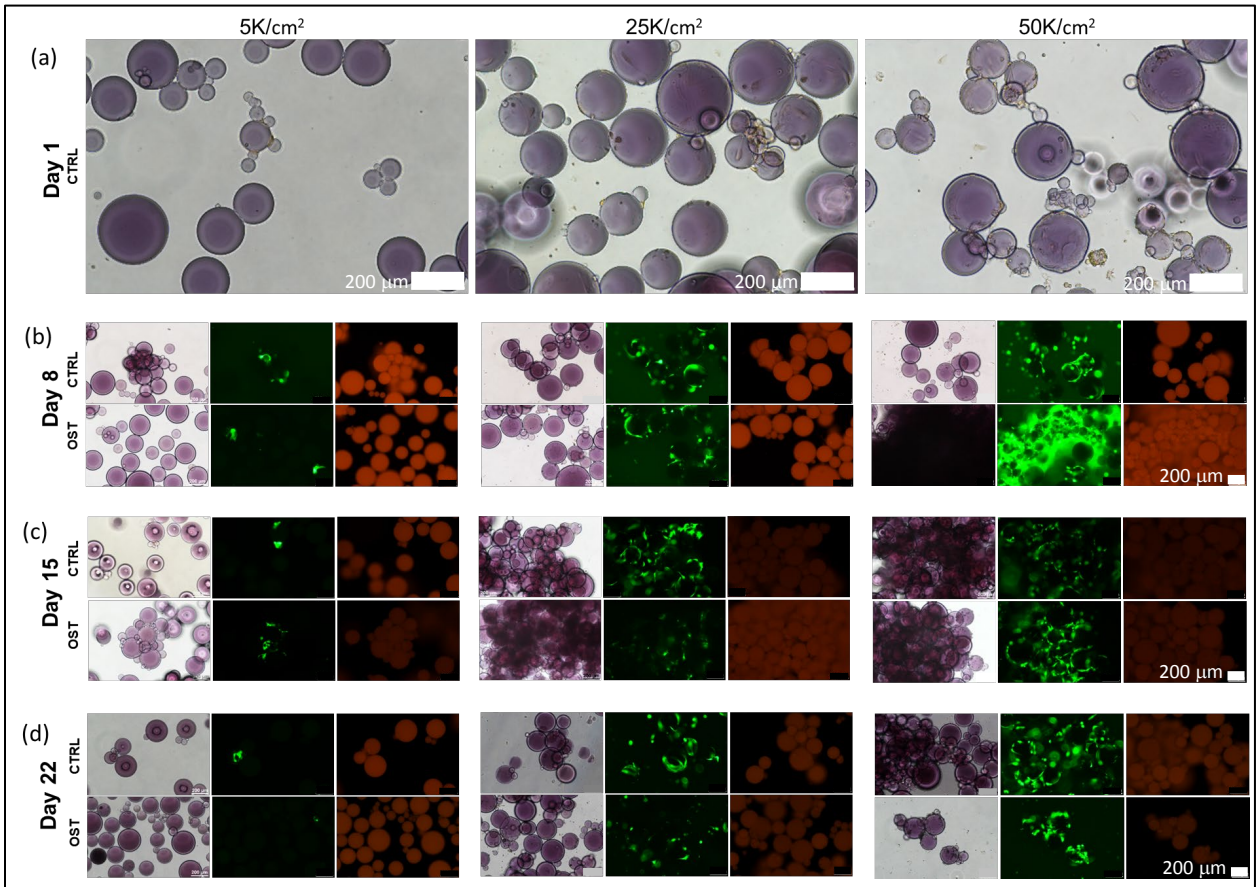

Figure 8: Optical microscopy images of MSC-laden gelatin microcarriers seeded at densities of 5,000 cells/cm², 25,000 cells/cm², and 50,000 cells/cm². Microcarriers were cultured for three weeks in packed beds in either control (CTRL) or osteogenic (OST) medium. Brightfield images were taken at a) day 1 after seeding, and brightfield and fluorescent images were subsequently taken at b) day 8, c) day 15, and d) day 22 after seeding. Vital staining shows the cytoplasm of living cells in green. The genipin-crosslinked gelatin matrix autofluoresces slightly in the red channel, but dead cells can be distinguished by red punctate nuclei. Scale bars represent 200 µm.

Cell viability was high at all cell densities and was maintained for the three-week culture period. The panels in Figure 8 show only a single cross-section of the sample, but it was confirmed that cell viability was uniform over the microcarriers. Cell viability was similarly high and uniform on the microcarriers under both control and osteogenic conditions. High cell viability has been observed previously using microcarrier culture [31, 65, 66]. The gelatin substrate, itself, is highly favorable for cell attachment, maintenance, and growth [67]. In addition to these features contributing to GmC cytocompatibility, the genipin crosslinker is known to be significantly less toxic than more common crosslinkers like glutaraldehyde and 1-ethyl-3-(3-dimethyl aminopropyl) carbodiimide [30]. Examination of the green-stained cytoplasm of the cells in **Figure 8** suggests

that MSC were able to attach and spread on the surface of microcarriers and at higher densities formed confluent layers that covered the surface. Previous studies have shown that attachment efficiency of cells to microcarriers is routinely high [28], and in the present study MSC seeding efficiency on 6.0 % gelatin microcarriers was >96% (**Supplemental Figure S4**). At this seeding efficiency, the average 177 μm diameter microcarrier would be expected to be seeded with approximately 15 cells per microcarrier on day 1 of culture, using a 15K cell/mL seeding density. The microcarrier format has the advantage that cells are exposed directly to the culture medium over a large surface area, allowing ready diffusion of nutrients, oxygen, and waste products, which in turn promotes high viability. In addition, dead cells will not adhere to the microcarrier surface and therefore will be washed away in the medium. These factors likely contribute to the very high viability of MSC on GmC observed in this study.

Figure 9 shows quantification of DNA extracted from packed beds of cultured Microcarriers over time, which provides an indicator of relative cell numbers. At day 1, the assayed cell numbers correlated in general with the initial seeding density for both CTRL and OST conditions. At the 5K/cm^2 and 25K/cm^2 seeding densities, cell number remained relatively constant over the culture period in control medium. At the 50K/cm^2 density, cell number declined over time in control medium and plateaued at a similar level to the samples with 25K/cm^2 initial seeding density. In contrast, cell number in osteogenic medium increased by day 8, but then fell back to a level similar to the samples with 25K/cm^2 initial seeding density at later time points. In general, there was little cell proliferation observed across the three week study period. This finding may be due to the use of the packed bed culture geometry, in which the relatively higher regional cell concentration may have inhibited cell proliferation, relative to less concentrated suspension culture. Similar findings have been found in prior work on culturing MSC on scaffolds in static culture, which was shown to enhance osteogenic markers, but decreased cell proliferation [68]. Similar rapid mineralization and matrix deposition was visible in the course of this study. Packed bed samples seeded at 25K/cm^2 and 50K/cm^2 in CTRL and OST conditions had fused completely by day 15, and this behavior was observed as early as day 8 in 50K/cm^2 samples. Taken together, these observations suggest a compounded osteogenic effect stemming from both the substrate material and culture method.

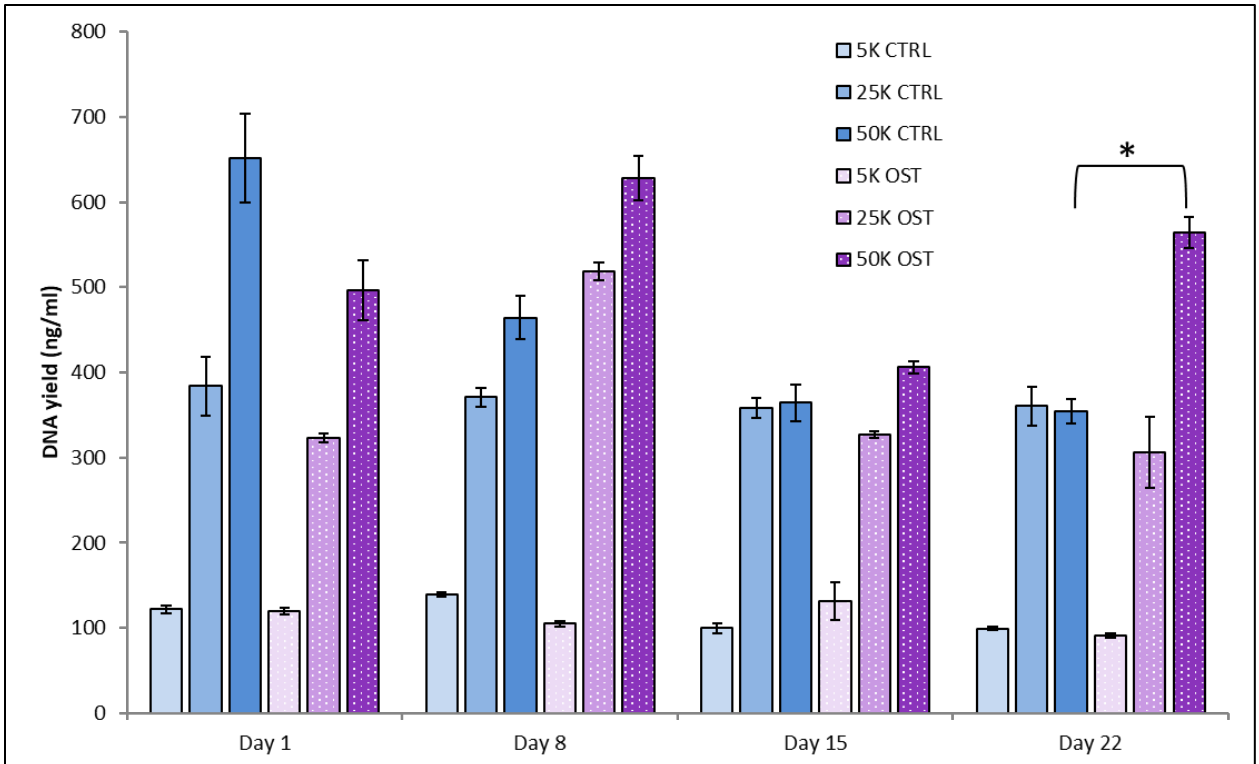

Figure 9: DNA content of gelatin microcarrier cultures over three weeks in control (CTRL) or osteogenic (OST) medium. Microcarriers were seeded at densities of 5,000 cells/cm^2, 25,000 cells/cm^2, or 50,000 cells/cm^2 on day 0. Brackets and associated stars indicate statistically significant differences ($p<0.05$).

Alkaline phosphatase (ALP) activity is an early marker of osteoblastic function and the process of matrix mineralization [69, 70]. **Figure 10** shows ALP activity of cells cultured on Microcarriers over time in response to control and osteogenic media, both in absolute terms (Fig. 10a) as well as normalized to DNA content (Fig. 10b). At the lowest cell seeding density (5K/cm^2), ALP activity did not change significantly over 3 weeks in culture in either control or osteogenic conditions. In contrast, at the higher seeding densities (25K/cm^2, 50K/cm^2) ALP activity increased significantly by day 8 and then returned to baseline levels. This effect was especially prominent in osteogenic culture and persisted when the data were normalized for DNA content, which is related to cell number.

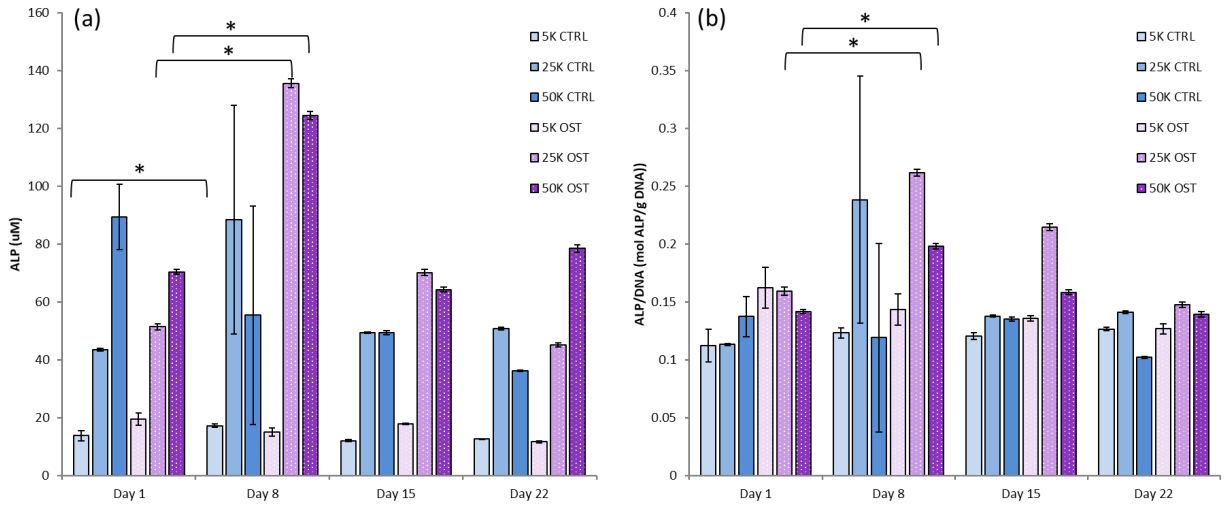

Figure 10: Quantification of alkaline phosphatase (ALP) activity of gelatin microcarrier cultures over three weeks in control (CTRL) or osteogenic (OST) medium. Microcarriers were seeded at densities of 5,000 cells/cm^2, 25,000 cells/cm^2, or 50,000 cells/cm^2 on day 0. ALP activity is expressed as a) absolute amount, and b) normalized relative to DNA content. Brackets and associated stars indicate statistically significant differences ($p<0.05$).

Calcium deposition is a direct indication of matrix mineralization and osteogenesis. **Figure 11** shows calcium deposition in Microcarriers cultures over time in response to control and osteogenic media, both in absolute terms (Fig. 11a) as well as normalized to DNA content (Fig. 11b). Calcium deposition generally increased over time in both control and osteogenic media, though the effect was markedly enhanced in osteogenic conditions. By day 15 and 22 in osteogenic medium, the 25K/cm^2 cultures had achieved 15.7-fold and 16.9-fold increases in calcium deposition, respectively, relative to day 1. The 50K/cm^2 cultures in osteogenic medium achieved 17.2-fold and 19.3-fold increases in calcium deposition, respectively, over the same time period. When

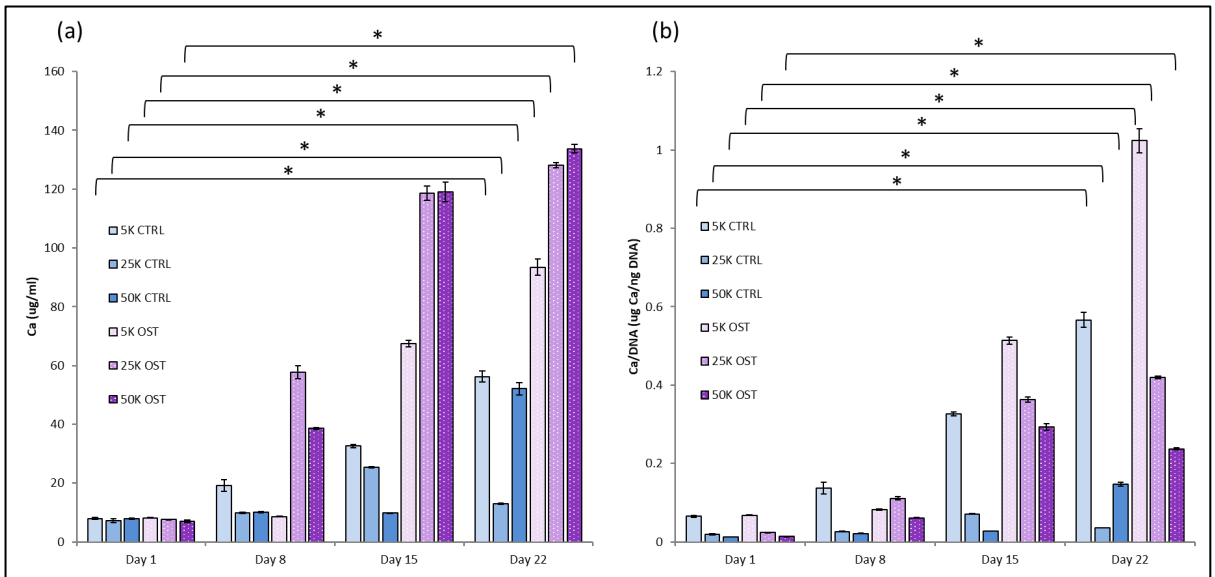

Figure 11: Quantification of calcium deposition (Ca) of gelatin microcarrier cultures over three weeks in control (CTRL) or osteogenic (OST) medium. Microcarriers were seeded at densities of 5,000 cells/cm^2, 25,000 cells/cm^2, or 50,000 cells/cm^2 on day 0. Calcium deposition is expressed as a) absolute amount, and b) normalized relative to DNA content. Brackets and associated stars indicate statistically significant differences ($p<0.05$).

normalized for DNA content, the general trends of increased calcium deposition over time were still pronounced; however the effect of cell density became evident. Low seeding density (5K/cm^2) resulted in higher relative calcium deposition per cell than higher cell densities by days 14 and 21, in both control and osteogenic media. In osteogenic medium, the amount of calcium deposited per cell was inversely related to the initial seeding density, suggesting that higher cell numbers have an inhibitory effect on matrix mineralization.

Conclusions

This study demonstrates that high yields of genipin-crosslinked gelatin microparticles can be reproducibly fabricated using a facile water-in-oil emulsification method. The size and size distribution of microparticle populations can be varied by controlling the impeller geometry, stirring rate, and concentration of gelatin. The mechanical properties of the matrix vary with gelatin concentration, with increasing concentrations resulting in stiffer matrices. Our studies show more specifically that a 6.0 % (wt/vol) microparticle used as a microcarrier for adult human MSC maintained high cell viability of attached cells over three weeks in culture in both control and osteogenic medium. The progenitor cells undergo osteogenic differentiation over time in culture, as evidenced by increased alkaline phosphatase activity and mineral deposition. The degree of osteogenesis is dependent on the initial seeding density of the microcarriers, with higher densities generally resulting in greater absolute osteogenic function. However, higher cell densities may also inhibit some aspects of matrix mineralization through a negative feedback effect. Taken together, these findings suggest that genipin-crosslinked GmC with a narrow size distribution are easily fabricated without the use of surfactant. The processed GmC support high cell attachment and viability, and are suitable substrates for the osteogenic differentiation of human progenitor cells. Such microcarriers are promising candidates for the culture and delivery of osteoprogenitor cell lines, and may have utility in regenerative medicine approaches to orthopedic tissue repair.

Acknowledgments

The authors gratefully acknowledge the technical assistance and guidance of their colleagues, and in particular Eric Hobson and Dr. Ramkumar Annamalai for technical assistance. This work was supported in part by the National Institute of Arthritis and Musculoskeletal and Skin Diseases (R01-AR062636, to JPS). CEN was partially supported by the Tissue Engineering and Regeneration Training Grant (T32-DE007057) at the University of Michigan. The content is solely the responsibility of the authors and does not necessarily represent the official views of the National Institutes of Health.

Author Disclosure Statement

No competing financial interests exist.

Data Availability Statement

The data that support the findings of this study are available from the corresponding author upon reasonable request.

Figure Captions

Figure 1: Schematic showing gelatin microcarrier production by water-in-oil emulsification and subsequent seeding with cells. Microcarriers in this study were composed of Type A gelatin crosslinked with genipin.

Figure 2: Comparative schematics of a) radial-bladed impeller and b) dual axial-bladed impellers. The axial-bladed impeller geometries used in this study differed only in blade cross-sectional dimensions, either 0.33 mm (Axial-0.3) or 1.0 mm (Axial-1.0).

Figure 3: Effect of impeller geometry on microparticle size using a stirring rate of 500 rpm. Upper panels show brightfield optical microscopy and batch-to-batch size distribution of microparticles formed by a) radial-blade, b) 0.33 mm diameter axial-blade, and c) 1.0 mm diameter axial-blade impeller geometries. Aggregate data are presented as d) representative size distributions, and e) median ± standard deviation for each impeller geometry.

Figure 4: Effect of stirring rate on gelatin microparticle size using the Axial-1.0 impeller geometry. Upper panels show brightfield optical microscopy of microparticles formed at a) 250 rpm, b) 380 rpm, and c) 500 rpm stirring rates. Aggregate data are presented as d) representative size distributions, and e) median ± standard deviation for each stirring rate.

Figure 5: Effect of stirring rate on gelatin microparticle size using the Axial-0.3 impeller geometry. Upper panels show brightfield optical microscopy of microparticles formed at a) 250 rpm, b) 380 rpm, and c) 500 rpm stirring rates. Aggregate data are presented as d) representative size distributions, and e) median ± standard deviation for each stirring rate.

Figure 6: Effect of gelatin concentration on gelatin microparticle size using the Axial-0.3 impeller at 500 rpm. Upper panels show brightfield optical microscopy of microparticles formed at a) 6.0 % wt/vol, b) 10.0 % wt/vol, and c) 14.0 % wt/vol gelatin. Aggregate data are presented as d) representative size distributions, and e) median ± standard deviation for each gelatin concentration.

Figure 7: Mechanical properties of gelatin formulations determined using shear rheometry. Genipin-crosslinked gelatin materials were analyzed to determine the a) storage modulus, b) loss modulus, and c) effect of strain amplitude for formulations of 6.0, 10.0, and 14.0 % wt/vol. Brackets and associated stars indicate statistically significant differences ($p<0.05$).

Figure 8: Optical microscopy images of MSC-laden gelatin microcarriers seeded at densities of 5,000 cells/cm^2, 25,000 cells/cm^2, and 50,000 cells/cm^2. Microcarriers were cultured for three weeks in packed beds in either control (CTRL) or osteogenic (OST) medium. Brightfield images were taken at a) day 1 after seeding, and brightfield and fluorescent images were subsequently taken at b) day 8, c) day 15, and d) day 22 after seeding. Vital staining shows the cytoplasm of living cells in green. The genipin-crosslinked gelatin matrix autofluoresces slightly in the red channel, but dead cells can be distinguished by red punctate nuclei. Scale bars represent 200 μm.

Figure 9: DNA content of gelatin microcarrier cultures over three weeks in control (CTRL) or osteogenic (OST) medium. Microcarriers were seeded at densities of 5,000 cells/cm^2, 25,000

cells/cm^2, or 50,000 cells/cm^2 on day 0. Brackets and associated stars indicate statistically significant differences ($p<0.05$).

Figure 10: Quantification of alkaline phosphatase (ALP) activity of gelatin microcarrier cultures over three weeks in control (CTRL) or osteogenic (OST) medium. Microcarriers were seeded at densities of 5,000 cells/cm^2, 25,000 cells/cm^2, or 50,000 cells/cm^2 on day 0. ALP activity is expressed as a) absolute amount, and b) normalized relative to DNA content. Brackets and associated stars indicate statistically significant differences ($p<0.05$).

Figure 11: Quantification of calcium deposition (Ca) of gelatin microcarrier cultures over three weeks in control (CTRL) or osteogenic (OST) medium. Microcarriers were seeded at densities of 5,000 cells/cm^2, 25,000 cells/cm^2, or 50,000 cells/cm^2 on day 0. Calcium deposition is expressed as a) absolute amount, and b) normalized relative to DNA content. Brackets and associated stars indicate statistically significant differences ($p<0.05$).

Figure S1: Effect of stirring rate on microparticle size using the Axial-1.0 impeller geometry, demonstrating very good batch-to-batch reproducibility. Histograms show three separate batches of microparticles at each stirring rate of a) 250 rpm, b) 380 rpm, and c) 500 rpm.

Figure S2: Effect of stirring rate on microparticle size using the Axial-0.3 impeller geometry, demonstrating very good batch-to-batch reproducibility. Histograms show three separate batches of microparticles at each stirring rate of a) 250 rpm, b) 380 rpm, and c) 500 rpm.

Figure S3: Fluorescence microscopy of human lung fibroblasts cultured on GmC at day 1 after seeding. Image at left shows green cytoplasm of living cells under control conditions. Image at right shows red-stained nuclei of dead cells after 20 min of ethanol treatment, showing that dead nuclei can be clearly distinguished from the autofluorescence of the gelatin matrix. Scale bar represents 200 μm.

Figure S4: Cell loading efficiency for MSC seeded at 15,000 cells/cm^2 on microcarriers of 6.0 %, 10.0 %, or 14.0 % wt/vol gelatin at day one after seeding.

Figure S5: Cell density on GMC over time of MSC seeded at 5,000-50,000 cells/cm^2 on 6.0 % wt/vol gelatin GmC and cultured in control and osteogenic media.

References Cited

1 Roberts TT, Rosenbaum AJ. Bone grafts, bone substitutes and orthobiologics: the bridge between basic science and clinical advancements in fracture healing. *Organogenesis*. 2012; **8**: 114-124.

2 Fernandez de Grado G, Keller L, Idoux-Gillet Y, Wagner Q, Musset AM, Benkirane-Jessel N, Bornert F, Offner D. Bone substitutes: a review of their characteristics, clinical use, and perspectives for large bone defects management. *J. Tissue Eng.* 2018; **9**: 1-18.

3 Verrier S, Alini M, Alsberg E, Buchman SR, Kelly D, Laschke MW, Menger MD, Murphy WL, Stegemann JP, Schütz M, Miclau T. Tissue engineering and regenerative approaches to improving the healing of large bone defects. *Eur. Cell Mater.* 2016; **32**: 87-110.

4 Perez JR, Kouroupis D, Li DJ, Best TM, Kaplan L, Correa D. Tissue engineering and cell-based therapies for fractures and bone defects. *Front. Bioeng. Biotechnol.* 2018; **6**: 105.

5 Lin H, Sohn J, Shen H, Langhans MT, Tuan RS. Bone marrow stem cells: Aging and tissue engineering applications to enhance bone healing. *Biomaterials.* 2019; **203**: 96-110.

6 Sobacchi C, Erreni M, Strina D, Palagano E, Villa A, Menale C. 3D bone biomimetic scaffolds for basic and translational studies with mesenchymal stem cells. *Int. J. Mol. Sci.* 2018; **19(10)**: 3150.

7 Pajarinen J, Lin T, Gibon E, Kohno Y, Maruyama M, Nathan K, Lu L, Yao Z, Goodman SB. Mesenchymal stem cell-macrophage crosstalk and bone healing. *Biomaterials*. 2019; **196**: 80-89.

8 Humbert P, Brennan MA, Davison N, Rosset P, Trichet V, Blanchard F, Layrolle P. Immune modulation by transplanted calcium phosphate biomaterials and human mesenchymal stromal cells in bone regeneration. *Front. Immunol.* 2019; **10**: 663.

9 Presen DM, Traweger A, Gimona M, Redl H. Mesenchymal stromal cell-based bone regeneration therapies: From cell transplantation and tissue engineering to therapeutic secretomes and extracellular vesicles. *Front. Bioeng. Biotechnol*. 2019; **7**: 352.

10 Rao RR, Stegemann JP. Cell-based approaches to the engineering of vascularized bone tissue. *Cytotherapy.* 2013; **15(11)**: 1309-1322.

11 Chen AKL, Reuveny S, Oh SKW. Application of human mesenchymal and pluripotent stem cell microcarrier cultures in cellular therapy: achievements and future direction. *Biotechnol. Adv.* 2013; **31**: 1032-1046.

12 Kim HW, Yoon BH, Kim HE. Microsphere of apatite-gelatin nanocomposite as bone regenerative filler. *J. Mater. Sci.: Mater. Med.* 2005; **16**: 1105-1109.

13 Nweke CE, Stegemann JP. Modular microcarrier technologies for cell-based bone regeneration. *J. Mater. Chem. B.* 2020; **8(18)**: 3972-3984.

14 Rao RR, Vigen ML, Peterson AW, Caldwell DJ, Putnam AJ, Stegemann JP. Dual-phase osteogenic and vasculogenic engineered tissue for bone formation. *Tissue Eng. Part A*. 2015; **21(3-4)**: 530-540.

15 Chao SC, Wang MJ, Pai NS, Yen SK. Preparation and characterization of gelatin–hydroxyapatite composite microspheres for hard tissue repair. *Mater. Sci. Eng. C*. 2015; **57**: 113-122.

16 Petruskevicius J, Nielsen S, Kaalund S, Knudsen PR, Overgaard S. No effect of Osteoset®, a bone graft substitute, on bone healing in humans: A prospective randomized double-blind study. *Acta Orthop. Scand.* 2002; **73**: 575-578.

17 Chen XY, Chen JY, Tong XM, Mei JG, Chen YF, Mou XZ. Recent advances in the use of microcarriers for cell cultures and their ex vivo and in vivo applications. *Biotechnol. Lett.* 2020; **42(1)**: 1-10.

18 Ornelas-Gonzalez A, Gonzalez-Gonzalez M, Rito-Palomares M. Microcarrier-based stem cell bioprocessing: GMP-grade culture challenges and future trends for regenerative medicine. *Crit. Rev. Biotechnol.* 2021; 1-15.

19 Saltz A, Kandalam U. Mesenchymal stem cells and alginate microcarriers for craniofacial bone tissue engineering: A review. *J. Biomed. Mater. Res. B.* 2016; **104(5)**: 1276-1284.

20 Shadjou N, Hasanzadeh M. Silica-based mesoporous nanobiomaterials as promoter of bone regeneration process. *J. Biomed. Mater. Res. B.* 2015; **103(11)**: 3703-3716.

21 Ghomi ER, Nourbaksh N, Kenari MA, Zare M, Ramakrishna S. Collagen-based biomaterials for biomedical applications. *J. Biomed. Mater. Res. B.* 2021.

22 Ballouze R, Marahat MH, Mohamad S, Saidin NA, Kasim SR, Ooi JP. Biocompatible magnesium-doped biphasic calcium phosphate for bone regeneration. *J. Biomed. Mater. Res. B.* 2021.

23 Hsu FY, Chueh SC, Wang YJ. Microspheres of hydroxyapatite/reconstituted collagen as supports for osteoblast cell growth. *Biomaterials*. 1999; **20**: 1931-1936.

24 Bliatsiou C, Malik A, Böhm L, and M. Kraume. Influence of impeller geometry on hydromechanical stress in stirred liquid/liquid dispersions. *Ind. Eng. Chem. Res*. 2018; **58(7)**: 2537-2550.

25 Goncharenko AV, Kotlyarova MS, Moisenovich AM, Arkhipova AY, Kulikov DA, Konkov AS, Kulikov AV, Mashkov AE, Agapov II, Moisenovich MM, Kirpichnikov MP. *Doklady Biochemistry and Biophysics*. Pleiades Publishing. 2017; 345-348.

26 Barrias CC, Ribeiro CC, Lamghari M, Miranda CS, Barbosa MA. Proliferation, activity, and osteogenic differentiation of bone marrow stromal cells cultured on calcium titanium phosphate microspheres. *J. Biomed. Mater. Res., Part A.* 2005; **72(1)**: 57-66.

27 Overstreet M, Sohrabi A, Polotsky A, Hungerford DS, Frondoza CG. Collagen microcarrier spinner culture promotes osteoblast proliferation and synthesis of matrix proteins. *In Vitro Cell. Dev. Biol. Animal*. 2003; **39**: 228-234.

28 Sart S, Errachid A, Schneider YJ, Agathos SN. Modulation of mesenchymal stem cell actin organization on conventional microcarriers for proliferation and differentiation in stirred bioreactors. *J. Tissue Eng. Regen. Med.* 2013; **7**: 537-551.

29 Yang Y, Rossi FM, Putnins EE. Ex vivo expansion of rat bone marrow mesenchymal stromal cells on microcarrier beads in spin culture. *Biomaterials*. 2007; **28**: 3110-3120.

30 Perez RA, Riccardi K, Altankov G, Ginebra MP. Dynamic cell culture on calcium phosphate microcarriers for bone tissue engineering applications. *J. Tissue Eng.* 2014; **5**: 2041731414543965.

31 Lau TT, Wang C, Wang DA. Cell delivery with genipin crosslinked gelatin microspheres in hydrogel/microcarrier composite. *Compos. Sci. Technol.* 2010; **70(13)**: 1909-1914.

32 Lau TT, Wang C, Peng SW, Su K, and Wang DA. Genipin-crosslinked microcarriers mediating hepatocellular aggregates formation and functionalities. J Biomed Mater Res A 2010; **96(1):** 204-211.

33 Lau TT, Lee LQP, Leong W, and Wang DA. Formation of model hepatocellular aggregates in a hydrogel scaffold using degradable genipin crosslinked gelatin microspheres as cell carriers. Biomed Mater 2012; **7:** 065003.

34 Solorio L, Zwolinski C, Lund AW, Farrell MJ, Stegemann JP. Gelatin microspheres crosslinked with genipin for local delivery of growth factors. *J. Tissue Eng. Regen. Med.* 2010; **4(7)**: 514-523.

35 Turner PA, Thiele JS, Stegemann JP. Growth factor sequestration and enzyme-mediated release from genipin-crosslinked gelatin microspheres. *J. Biomaterials Sci., Polym. Ed.* 2017; **28**: 1826-1846.

36 Annamalai RT, Turner PA, Carson IV WF, Levi B, Kunkel S, Stegemann JP. Harnessing macrophage-mediated degradation of gelatin microspheres for spatiotemporal control. *Biomaterials.* 2018; **161**: 216-227.

37 Vo TN, Shah SR, Lu S, Tatara AM, Lee EJ, Roh TT, Tabata Y, Mikos AG. Injectable dual-gelling cell-laden composite hydrogels for bone tissue engineering. *Biomaterials.* 2016; **83**: 1-11.

38 Kim HW, Gu HJ, Lee HH. Microspheres of Collagen-Apatite Nanocomposites with Osteogenic Potential for Tissue Engineering. *Tissue Eng*. 2007; **13**: 965-973.

39 Luetchford KA, Chaudhuri JB, Paul A. Silk fibroin/gelatin microcarriers as scaffolds for bone tissue engineering. *Mater. Sci. Eng. C.* 2020; **106**: 110116.

40 Shen S, Fu D, Xu F, Long T, Hong F, Wang J. The design and features of apatite-coated chitosan microspheres as injectable scaffold for bone tissue engineering. *Biomed. Mater*. 2013; **8**: 025007.

41 Annamalai RT, Hong X, Schott NG, Tiruchinapally G, Levi B, Stegemann JP. Injectable osteogenic microtissues containing mesenchymal stromal cells conformally fill and repair critical-size defects. *Biomaterials*. 2019; **208**: 32-44.

42 Perez RA, Del Valle S, Altankov G, Ginebra MP. Porous hydroxyapatite and gelatin/hydroxyapatite microspheres obtained by calcium phosphate cement emulsion. *J. Biomed. Mater. Res. Part B Appl. Biomater.* 2011; **97(1)**: 156-166.

43 Cuzmar E, Perez RA, Manzanares MC, Ginebra MP, Franch J. In vivo osteogenic potential of biomimetic hydroxyapatite/collagen microspheres: comparison with injectable cement pastes. *PLoS One*. 2015; **10(7)**: e0131188.

44 Hsu FY, Tsai SW, Lan CW, Wang YJ. An in vivo study of a bone grafting material consisting of hydroxyapatite and reconstituted collagen. *J. Mater. Sci.: Mater. Med.* 2005; **16(4)**: 341-345.

45 Dosta P, Ferber S, Zhang Y, Wang K, Ros A, Uth N, Levinson Y, Abraham E, Artzi N. Scale-up manufacturing of gelatin-based microcarriers for cell therapy. *J Biomed Mater Res B Appl Biomater*. 2020; **108**: 2937-2949.

46 Hayashi K, Tabata Y. Preparation of stem cell aggregates with gelatin microspheres to enhance biological functions. *Acta Biomater.* 2011; **7**: 2797-2803.

47 Yang G, Xiao Z, Long H, Ma K, Zhang J. Assessment of the characteristics and biocompatibility of gelatin sponge scaffolds prepared by various crosslinking methods. *Sci. Rep.* 2018; **8(1)**: 1-3.

48 Annamalai RT, Naik T, Prout H, Putnam AJ, and Stegemann JP. Biofabrication of injectable fibrin microtissues for minimally-invasive therapies: application of surfactants. Biomed Mater 2018; **13(4):** 045005.

49 Hwang YJ, Larsen J, Krasieva TB, Lyubovitsky JG. Effect of genipin crosslinking on the optical spectral properties and structures of collagen hydrogels. *ACS Appl. Mat. & Interfaces*. 2011; **3**: 2579-2584.

50 Babur BK, Futrega K, Lott WB, Klein TJ, Cooper-White J, Doran MR. High-throughput bone and cartilage micropellet manufacture, followed by assembly of micropellets into biphasic osteochondral tissue. *Cell Tissue Res.* 2015; **361**: 755-768.

51 Saito E, Suarez-Gonzalez D, Rao RR, Stegemann JP, Murphy WL, Hollister SJ. Use of micro-computed tomography to nondestructively characterize biomineral coatings on solid freeform fabricated poly (L-lactic acid) and polycaprolactone scaffolds in vitro and in vivo. *Tissue Eng. Part C Methods.* 2013; **19(7)**: 507-517.

52 Man W, Donev A, Stillinger FH, Sullivan MT, Russel WB, Heeger D, Inati S, Torquato S, Chaikin PM. Experiments on random packings of ellipsoids. *Phys. Rev. Lett*. 2005; **94**: 198001.

53 Baule A, Makse HA. Fundamental challenges in packing problems: from spherical to non-spherical particles. *Soft Matter*. 2014; **10**: 4423-4429.

54 Shapoff CA, Bowers GM, Levy B, Mellonig JT, Yukna RA. The effect of particle size on the osteogenic activity of composite grafts of allogeneic freeze-dried bone and autogenous marrow. *J. Periodontol.* 1980; **29**: 33-41.

55 Leiblein M, Koch E, Winkenbach A, Schaible A, Nau C, Buchner H, Schroder K, Marzi I, Henrich D. Size matters: Effect of granule size of the bone graft substitute (Herafill®) on bone healing using Masquelet's induced membrane in a critical size defect model in the rat's femur. *J. Biomed. Mater. Res. Part B Appl. Biomater.* 1980; **29**: 33-41.

56 Handorf AM, Zhou Y, Halanski MA, Li WJ. Tissue stiffness dictates development, homeostasis, and disease progression. *Organogenesis*. 2015; **11(1)**: 1-15.

57 Vining KH, Mooney DH. Mechanical forces direct stem cell behavior in development and regeneration. *Nat. Rev. Mol. Cell Biol.* 2017; **18**: 728-742.

58 Butcher DT, Alliston T, Weaver VM. A tense situation: forcing tumour progression. *Nat. Rev. Cancer.* 2009; **9**: 108-122.

59 Cox TR, Erler JT. Remodeling and homeostasis of the extracellular matrix: implications for fibrotic diseases and cancer. *Dis. Model. Mech.* 2011; **4(2)**: 165-178.

60 Ruiz SA, Chen CS. Emergence of patterned stem cell differentiation within multicellular structures. *Stem Cells*, 2008; **26**: 2921-2927.

61 Engler AJ, Sen S, Sweeney HL, Discher DE. Matrix elasticity directs stem cell lineage specification. *Cell*. 2006; **126**: 677-689.

62 Lin L, Regenstein JM, Lv S, Lu J, Jiang S. An overview of gelatin derived from aquatic animals: Properties and modification. *Trends Food Sci. Technol.* 2017; **68**: 102-112.

63 Nathia-Neves G, Meireles MAA. Genipap: A New Perspective on Natural Colorants for the Food Industry. *Food Public Health.* 2018; **8(1)**: 21-33.

64 Cho YJ, Kim SY, Kim J, Choe EK, Kim SI, Shin HJ. One-Step Enzymatic Synthesis of Blue Pigments from Geniposide for Fabric Dyeing. *Biotechnol. Bioprocess Eng.* 2006; **11**: 230-234.

65 Wissemann KW, Jacobson BS. Pure gelatin microcarriers: synthesis and use in cell attachment and growth of fibroblast and endothelial cells. *In vitro Cellular & Dev. Biology*. 1985; **21**: 391-401.

66 Yao L, Phan F, Li Y. Collagen microsphere serving as a cell carrier supports oligodendrocyte progenitor cell growth and differentiation for neurite myelination in vitro. *Stem Cell Res. Ther.* 2013; **4**: 109.

67 Bello AB, Kim D, Kim D, Park H, Lee SH. Engineering and functionalization of gelatin biomaterials: From cell culture to medical applications. *Tissue Eng. Part B: Rev.* 2020; **26**: 2.

68 Tsai HH, Yang KC, Wu MH, Chen JC, Tseng CL. The effects of different dynamic culture systems on cell proliferation and osteogenic differentiation in human mesenchymal stem cells. *Int. J. Mol. Sci.* 2019; **20(16)**: 4024.

69 Vimalraj S. Alkaline phosphatase: Structure, expression and its function in bone mineralization. *Gene.* 2020; **754**: 144855.

70 Tseng PC, Young TH, Wang TM, Peng HW, Hou SM, Yen ML. Spontaneous osteogenesis of MSCs cultured on 3D microcarriers through alteration of cytoskeletal tension. *Biomaterials.* 2011; **33(2)**: 556-564.

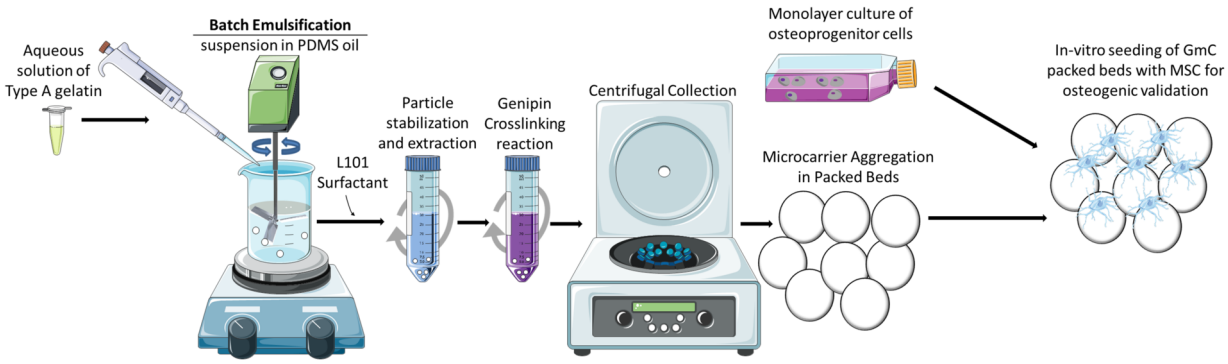

JBMB_34998_Fig 1.tif

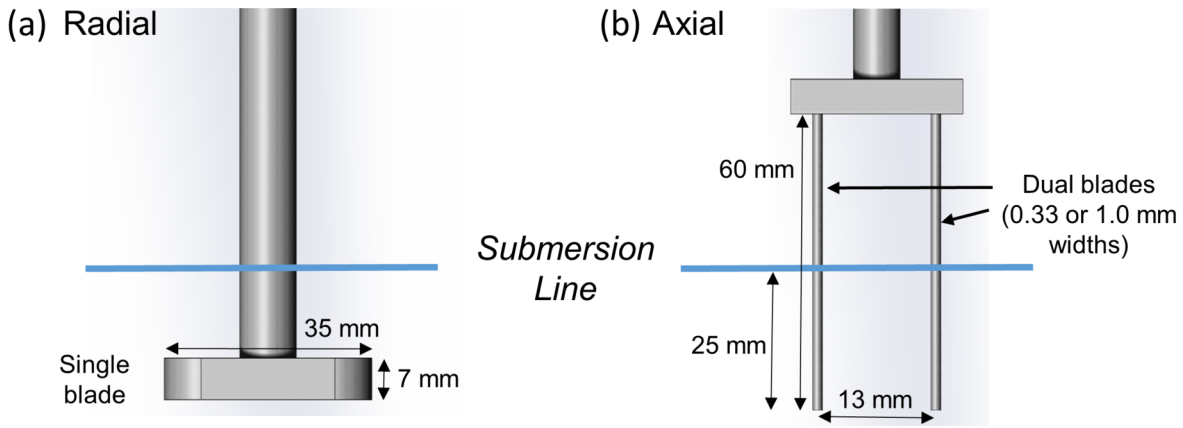

JBMB_34998_Fig 2.tif

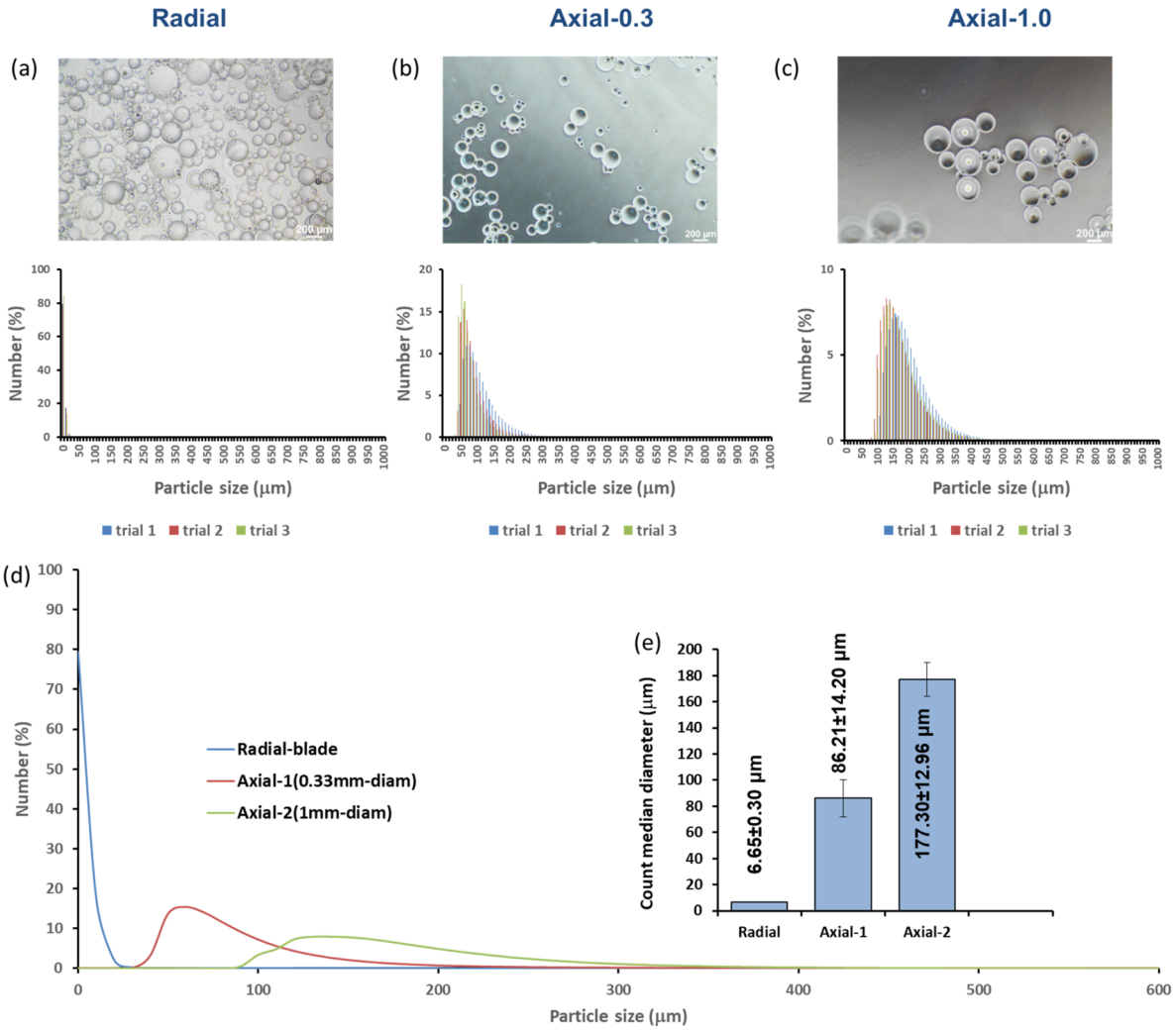

JBMB_34998_Fig 3.tif

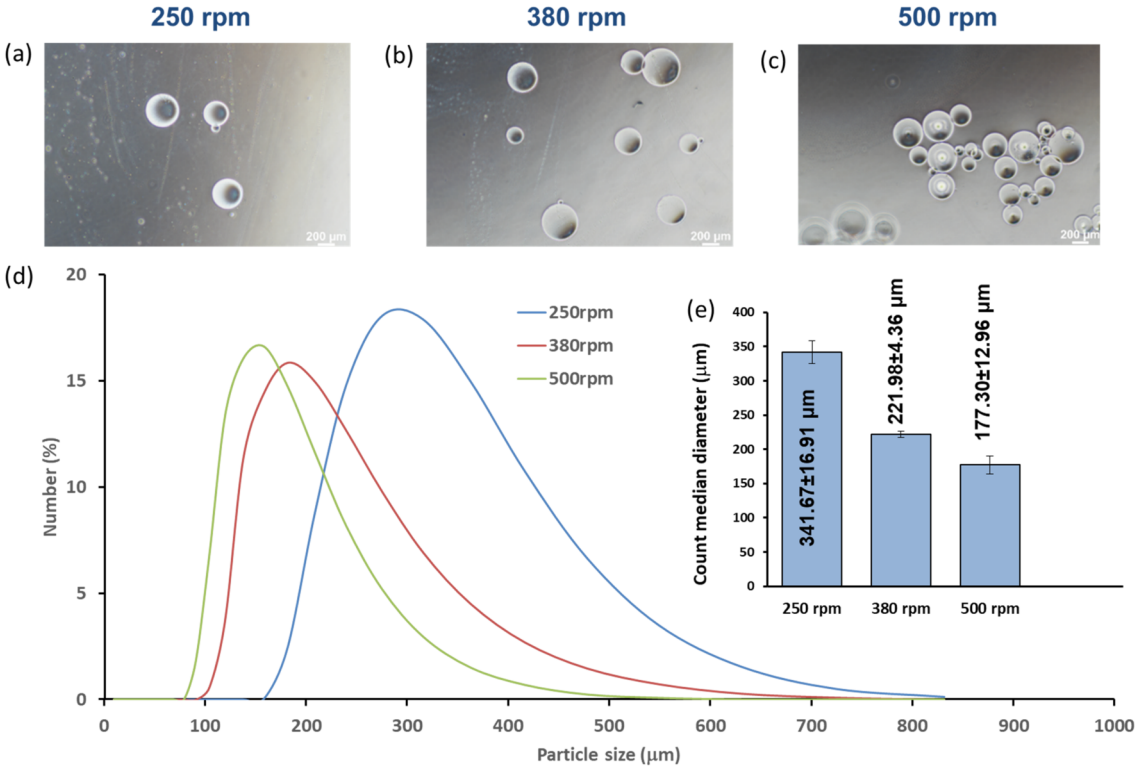

JBMB_34998_Fig 4.tif

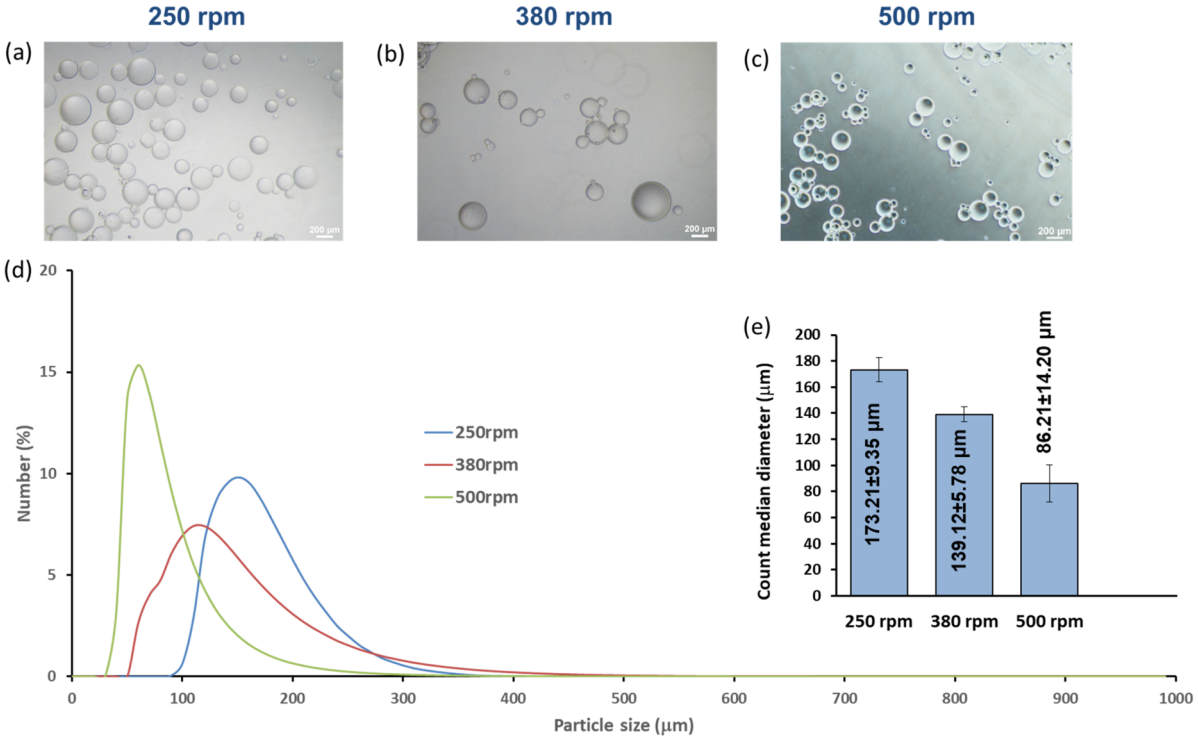

JBMB_34998_Fig 5.tif

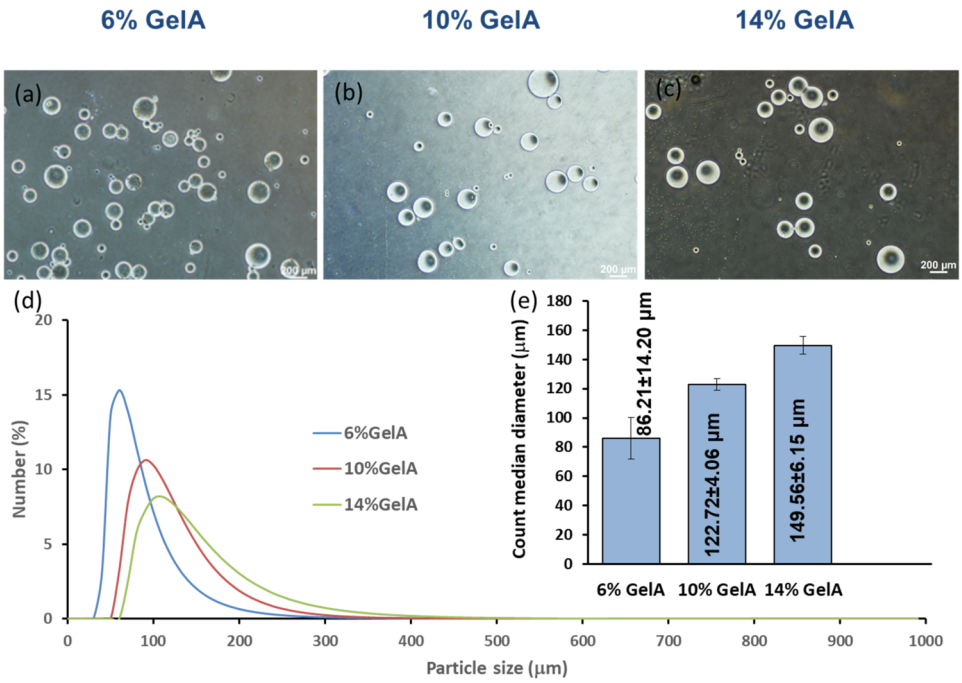

JBMB_34998_Fig 6.tif

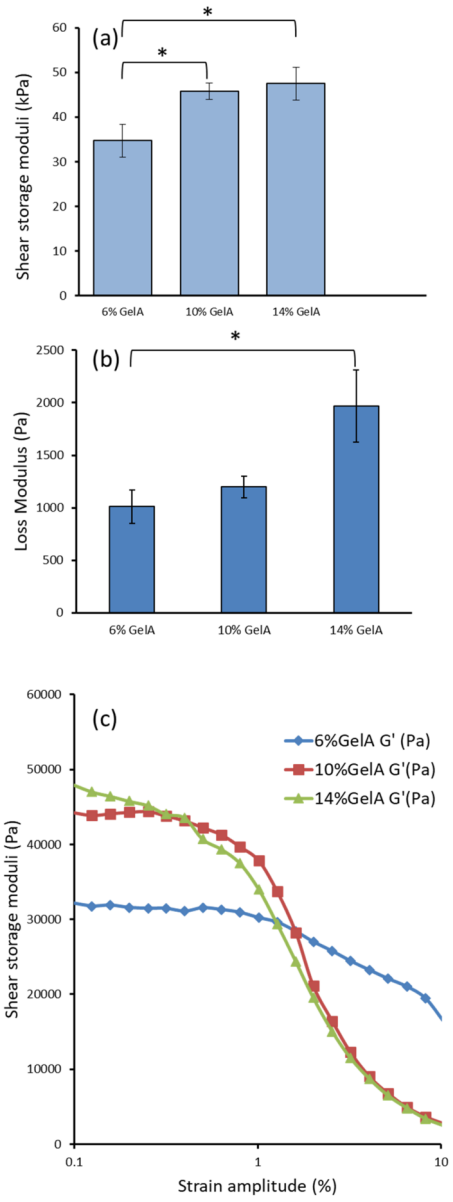

JBMB_34998_Fig 7.tif

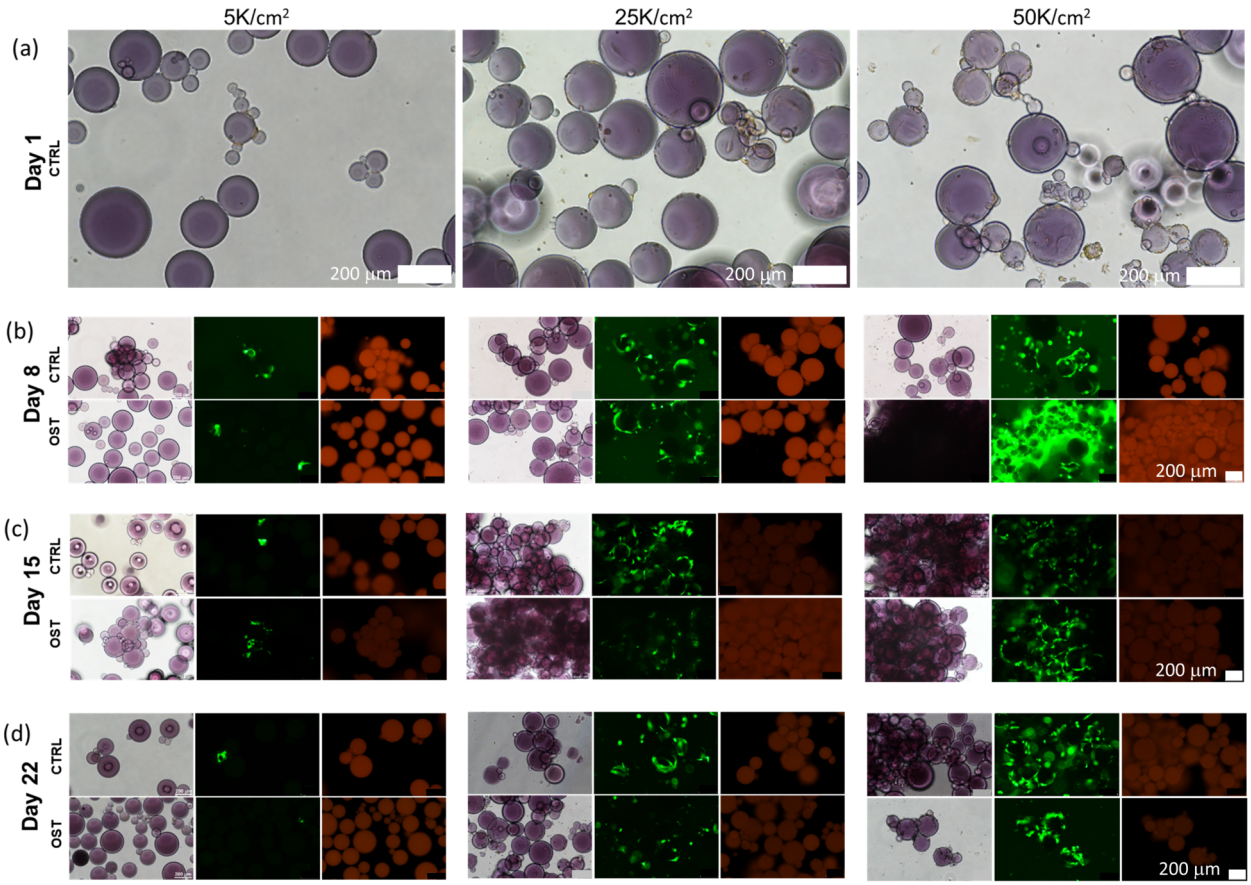

JBMB_34998_Fig 8.tif

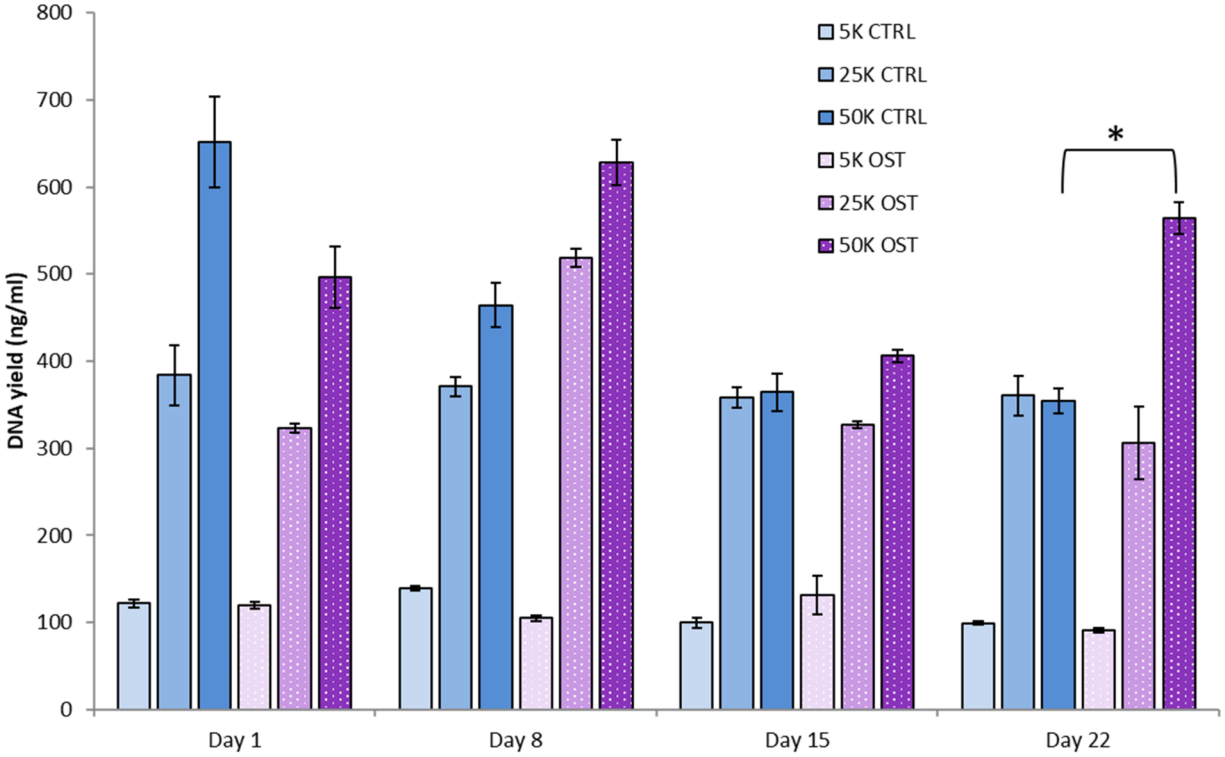

JBMB_34998_Fig 9.tif

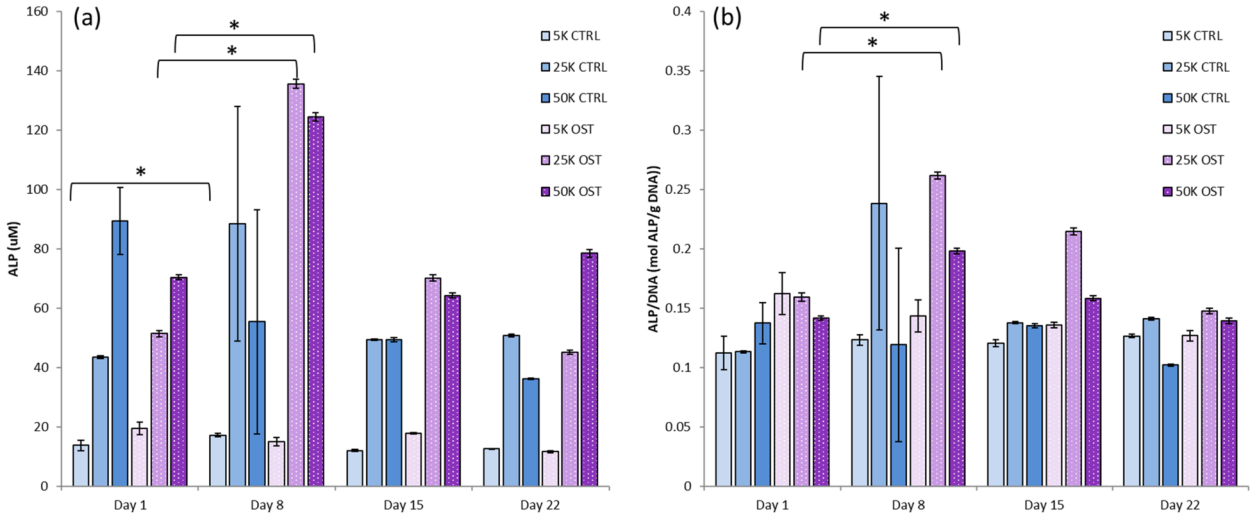

JBMB_34998_Fig 10.tif